



ORIGINAL ARTICLE

The synthesis, characterizations, and lead adsorption studies of chicken eggshell powder and chicken eggshell powder-doped iron (III) oxide-hydroxide



Pornsawai Praipipat^{a,b,*}, Pimploy Ngamsurach^{a,b}, Krissana Pratumkaew^a

^a Department of Environmental Science, Faculty of Science, Khon Kaen University, Khon Kaen 40002, Thailand

^b Environmental Applications of Recycled and Natural Materials (EARN) Laboratory, Khon Kaen University, Khon Kaen 40002, Thailand

Received 24 October 2022; accepted 28 January 2023

Available online 3 February 2023

KEYWORDS

Food waste;
Metal oxide;
Adsorption;
Heavy metal;
Wastewater treatment

Abstract The contamination of lead in wastewater causes water quality problems, which is toxic to aquatic organisms and environment, so wastewater treatment is required before discharging to receiving water. Chicken eggshell powder (CP) and chicken eggshell powder-doped iron (III) oxide-hydroxide (CPF) were synthesized, characterized, and investigated lead removal efficiencies by batch experiments, adsorption isotherms, kinetics, and desorption experiments. The specific surface area and pore volume of CPF were higher than CP, whereas the pore diameter size of CPF was smaller than CP. The phase structures of both materials demonstrated semi-crystalline phases with presenting peaks of calcium carbonate. Their surface morphologies were irregular, rough, and uneven surfaces. In both materials, they detected carbon, calcium, oxygen, O—H, N—H, C=O, C—O, and C—H. The point of zero charges (pH_{pzc}) of CP and CPF were 4.47 and 4.83. For batch experiments, CPF demonstrated a higher lead removal efficiency than CP because of spending less material dosage and contact time than CP, and both materials had high lead removals at a lead concentration of 50 mg/L by more than 95 %. Thus, the addition of iron (III) oxide-hydroxide helped to increase material efficiency for lead adsorption. CP corresponded to the Langmuir model while CPF corresponded to the Freundlich model. In addition, both materials corresponded to a pseudo-second-order kinetic model relating to a chemisorption process. Moreover, both materials could be

* Corresponding author at: Department of Environmental Science, Faculty of Science, Khon Kaen University, Khon Kaen 40002, Thailand; Environmental Applications of Recycled and Natural Materials (EARN) Laboratory, Khon Kaen University, Khon Kaen 40002, Thailand.

E-mail addresses: pornprai@kku.ac.th (P. Praipipat), pimploy@kkumail.com (P. Ngamsurach), krissana@kkumail.com (K. Pratumkaew).
Peer review under responsibility of King Saud University.



Production and hosting by Elsevier

reusable for more than 5 cycles for lead adsorption of more than 77 %. Therefore, CPF was a potential material to apply for lead removals in industrial applications.

© 2023 The Author(s). Published by Elsevier B.V. on behalf of King Saud University. This is an open access article under the CC BY-NC-ND license (<http://creativecommons.org/licenses/by-nc-nd/4.0/>).

1. Introduction

Economic, industrial, and technological growth causes an increase in releasing pollutants into the environment resulted to create water pollution. Various types of pollutants such as nutrients, pesticides, dyes, pharmaceutical products, and heavy metals affect the water quality and aquatic environment including human health effects. Especially, heavy metals are the most concerned because of their persistence, bioaccumulation, and toxicity to aquatic organisms and the environment at low concentrations (Ali et al., 2019). Lead is a toxic heavy metal that is normally used in many manufacturing processes of pigment, battery, steel, and plastic industries (Obeng-Gyasi, 2019), so their effluents might have lead contaminated with the above concerns. Moreover, lead toxicity might cause human health effects on misfunctions in nerve, blood, respiration, and reproduction systems (Balali-Mood et al., 2021). Therefore, wastewater treatment is required for removing lead from wastewater to be below 0.02 mg/L following USEPA standards before discharging for a safe environment.

Many methods of chemical precipitation, oxidation–reduction, coagulation-flocculation, ion exchange, and reverse osmosis are generally used for heavy metal eliminations including a lead in wastewater; however, they had disadvantages of incomplete heavy metal removals, expensive operating costs, complicated operations, and creating a big load of toxic sludges (Qasem et al., 2021). While an adsorption method offers an effective method for lead removal with easy operation and suitable operation cost, and this method also is available several choices of adsorbents depending upon the contaminated target metal,

budget, and requirement of treated water quality. Several commercial, agricultural, industrial, and waste adsorbents are used for removing heavy metals, dyes, and antibiotics in wastewater such as activated carbon, zeolite, chitosan, rice husk, corn stalk, sawdust, bagasse, bagasse fly ash, coal fly ash, banana peels, lemon peels, pistachio shells, shrimp shells, and eggshells (Alnasrawi et al., 2022; Jangkorn et al., 2022; Kristianto et al., 2019; Mohammed et al., 2020; Mohammed and Kareem, 2021; Praipipat et al., 2022a, 2023a, 2023c; Tejada-Tovar et al., 2019; Threepanich and Praipipat, 2022; Praipipat et al., 2023). However, this study will focus on food waste because of its benefits as low-cost adsorbents used for improving water quality along with reducing waste volumes in terms of waste management and disposal. The elimination of heavy metals in wastewater from various food wastes in 2018–2022 is demonstrated in Table 1. Among those adsorbents, chicken eggshells are a good choice because it has good chemical properties of calcium carbonate (CaCO₃), carboxyl group (–COOH), and hydroxyl group (–OH) for lead adsorption in wastewater. Even though chicken eggshells have good chemical properties for lead adsorption, they also need to improve in case of high lead concentration for industrial applications.

Various metal oxides of titanium dioxide (TiO₂), aluminum oxide (Al₂O₃), zinc oxide (ZnO), iron (II or III) oxide (Fe₃O₄), and iron (III) oxide-hydroxide have been reported by previous studies for improving adsorbent efficiency by increasing surface area and adsorption capacity for heavy metal removals (Aryee et al., 2021; Mahdavi et al., 2015; Ngamsurach et al., 2022a; Praipipat et al., 2023b; Razzaz et al., 2016; Threepanich and Praipipat, 2021). Among those

Table 1 The elimination of heavy metals in wastewater from various food wastes.

Materials	Modifications	Heavy ions	q_m (mg/g)	references
Avocado seed	–	Pb(II)	18.90	(Boeykens et al., 2019)
Avocado seed	–	Cr(VI)	3.39	(Boeykens et al., 2019)
Avocado seed	Phosphoric acid (H ₃ PO ₄)	Pb (II)	26.60	(Boeykens et al., 2019)
Avocado seed	Phosphoric acid (H ₃ PO ₄)	Cr(VI)	5.10	(Boeykens et al., 2019)
Watermelon rind	–	Ni(II)	38.98	(Mathangi and Helen Kalavathy, 2019)
Cassava peel	–	Pb(II)	11.79	(Tejada-Tovar et al., 2019)
Banana peel	–	Pb(II)	18.96	(Tejada-Tovar et al., 2019)
Yam peel	–	Pb(II)	98.36	(Tejada-Tovar et al., 2019)
Pea peel	Biochar	Pb(II)	152.50	(Novoseltseva et al., 2021)
Sweet lemon peel	Biochar	Pb(II)	2840.91	(Kumar, 2020)
Potato peel	Activated carbon	Pb(II)	262	(Kyzas and Mitropoulos, 2018)
Soya bean	Sodium hydroxide (NaOH)	Pb(II)	0.72	(Gaur et al., 2018)
Soya bean	Sodium hydroxide (NaOH)	As(V)	0.08	(Gaur et al., 2018)
Pistachio shell	–	Cd(II)	51.28	(Kayranli, 2022)
Peanut shell	–	Cd(II)	62.11	(Kayranli, 2022)
Almond shell	–	Cd(II)	78.74	(Kayranli, 2022)
Walnut shell	Activated carbon	Cd(II)	14.00	(Mohseni et al., 2022)
Tea waste	–	Pb(II)	1.20	(Çelebi et al., 2020)
Tea waste	–	Cd(II)	2.47	(Çelebi et al., 2020)
Tea waste	–	Ni(II)	1.16	(Çelebi et al., 2020)
Tea waste	–	Zn(II)	1.46	(Çelebi et al., 2020)
Eggshell	–	Ni(II)	13.53	(Kristianto et al., 2019)
Eggshell	Calcined	Ni(II)	769.23	(Kristianto et al., 2019)
Eggshell	Biochar	As(V)	0.89	(Akram et al., 2022)
Eggshell	Potassium permanganate (KMnO ₄)	Pb(II)	709.13	(Basaleh et al., 2020)
Eggshell	Iron(II) sulfate (FeSO ₄)	Cd(II)	69.77	(Meng et al., 2022)

metal oxides, iron (III) oxide-hydroxide is an interesting choice for improving material efficiency with the advantages mentioned above, and it also is low cost, non-toxicity, and chemical stability in a wide pH (Attia et al., 2022; Xu et al., 2015). In previous studies, many studies have used eggshells for removing various heavy metals of cadmium (Cd^{2+}), copper (Cu^{2+}), arsenate (As^{5+}), mercury (Hg^{2+}), nickel (Ni^{2+}), zinc (Zn^{2+}), and lead (Pb^{2+}) with or without material modifications by the calcination process or adding iron (II or III) oxides of magnetite (Fe_3O_4) and iron (II) sulfate (FeSO_4) (Meng et al., 2022; Naghizadeh et al., 2018; Peigneux et al., 2020; Rahmani-Sani et al., 2020). However, no one used iron (III) oxide-hydroxide to modify eggshell adsorbent for eliminating lead (Pb^{2+}), so it is a good idea to investigate the chicken eggshell efficiency by adding iron (III) oxide-hydroxide for offering high adsorbent efficiency to deal high strength of heavy metals in industrial wastewater. Therefore, this study attempts to synthesize chicken eggshell powder materials with or without modification by iron (III) oxide-hydroxide, to compare their lead removal efficiencies through batch experiments, and verify whether adding metal oxide helped to improve material efficiency for lead adsorption.

This study aimed to synthesize chicken eggshell powder (CP) and chicken eggshell powder-doped iron (III) oxide-hydroxide (CPF), to characterize their specific surface area, pore volumes, pore sizes, crystalline structures, surface morphologies, chemical elements, and chemical functional groups by Brunauer-Emmett-Teller (BET), X-ray Diffractometer (XRD), Field Emission Scanning Electron Microscopy and Focus Ion Beam (FESEM-FIB) with Energy Dispersive X-ray Spectrometer (EDX), and Fourier Transform Infrared Spectroscopy (FT-IR), and to examine their lead removal efficiencies by batch experiments with varying doses, contact time, pH, and concentration. Finally, their lead adsorption patterns and mechanisms were studied by linear and nonlinear adsorption isotherms of Langmuir, Freundlich, Temkin, and Dubinin-Radushkevich models and kinetics of pseudo-first-kinetic, pseudo-second-kinetic, elovich, and intraparticle diffusion models. Finally, the material reusability was investigated through desorption experiments.

2. Materials and methods

2.1. Raw material

Chicken eggshells were collected from the local restaurants in Khon Kaen province, Thailand.

2.2. Chemicals

All chemicals were analytical grades (AR) without purification before use which were ferric chloride hexahydrate ($\text{FeCl}_3 \cdot 6\text{H}_2\text{O}$) (LOBA, India), sodium hydroxide (NaOH) (RCI Labscan, Thailand), sodium chloride (NaCl) (RCI Labscan, Thailand), hydrochloric acid (HCl) (RCI Labscan, Thailand), lead nitrate ($\text{Pb}(\text{NO}_3)_2$) (QRcC, New Zealand). For a pH adjustment, 1 % NaOH and 1 % HNO_3 were used.

2.3. Synthesis of chicken eggshell powder (CP) and chicken eggshell powder-doped iron (III) oxide-hydroxide (CPF)

The synthesis of CP and CPF are demonstrated in Fig. 1a-b which is based on Praipipat, P. et al (Praipipat et al., 2022b), and the details were clearly explained below:

2.3.1. The synthesis of CP

Chicken eggshells were washed with tap water to eliminate contaminations, and then they were dried overnight in a hot

air oven (Binder, FED 53, Germany) at 80 °C. Then, they were ground and sieved in size of 125 μm , and they were kept in a desiccator before use called chicken eggshell powder (CP).

2.3.2. The synthesis of CPF

5 g of CP were added to 500 mL of Erlenmeyer flask containing 160 mL of 5 % $\text{FeCl}_3 \cdot 6\text{H}_2\text{O}$, and they were mixed by an orbital shaker (GFL, 3020, Germany) of 200 rpm for 3 h. Then, they were filtrated and air-dried at room temperature for 12 h. After that, they were added to 500 mL of Erlenmeyer flask containing 160 mL of 5 % NaOH, and they were mixed by an orbital shaker of 200 rpm for 1 h. Then, they were filtered, air-dried at room temperature for 12 h, and kept in a desiccator before use called chicken eggshell powder-doped iron (III) oxide-hydroxide (CPF).

2.4. Characterizations of chicken eggshell powder (CP) and chicken eggshell powder-doped iron (III) oxide-hydroxide (CPF)

Brunauer-Emmett-Teller (BET) (Bel, Bel Sorp mini X, Japan), X-ray Diffractometer (XRD) (PANalytical, EMPYREAN, UK), Field Emission Scanning Electron Microscopy and Focus Ion Beam (FESEM-FIB) with Energy Dispersive X-ray Spectrometer (EDX) (FEI, Helios NanoLab G3 CX, USA, and Fourier Transform Infrared Spectroscopy (FT-IR) (Bruker, TENSOR27, Hong Kong) were used for characterizing the specific surface area, pore size, pore volume, surface morphology, chemical compositions, and chemical functional groups of CP and CPF.

2.5. The point of zero charges of chicken eggshell powder (CP) and chicken eggshell powder-doped iron (III) oxide-hydroxide (CPF)

The study of the point of zero charges of CP and CPF is based on the study of Praipipat, P. et al (Praipipat et al., 2022b). The sample solutions of 0.1 M NaCl were prepared in different pH values from 2 to 12 by using 0.1 M HCl and 0.1 M NaOH. Then, 0.1 g of material was added to 250 mL Erlenmeyer flasks containing 50 mL of each sample solution, and it was shaken by an orbital shaker (GFL, 3020, Germany) at room temperature at 150 rpm for 24 h. After that, the final pH value of the sample solution was measured by a pH meter (Mettler Toledo, SevenGo with InLab 413/IP67, Switzerland) and calculated ΔpH ($\text{pH}_{\text{final}} - \text{pH}_{\text{initial}}$). A point that is the crosses line of ΔpH versus $\text{pH}_{\text{initial}}$ equal to zero is the point of zero charge (pH_{pzc}) of material.

2.6. Batch adsorption experiments

The different values of dose (0.1 to 0.6 g), contact time (1 to 6 h), pH (1, 3, 5, 7, 9, 11), and concentration (10 to 70 mg/L) were applied for investigating lead removal efficiencies of chicken eggshell powder (CP) and chicken eggshell powder-doped iron (III) oxide-hydroxide (CPF) through a series of batch adsorption experiments which the control condition was the initial lead concentration of 50 mg/L, a sample volume of 200 mL, pH 5, a shaking speed of 200 rpm, and a temperature of 25 °C. The optimum value was selected from the lowest value of each affecting factor with the highest lead removal

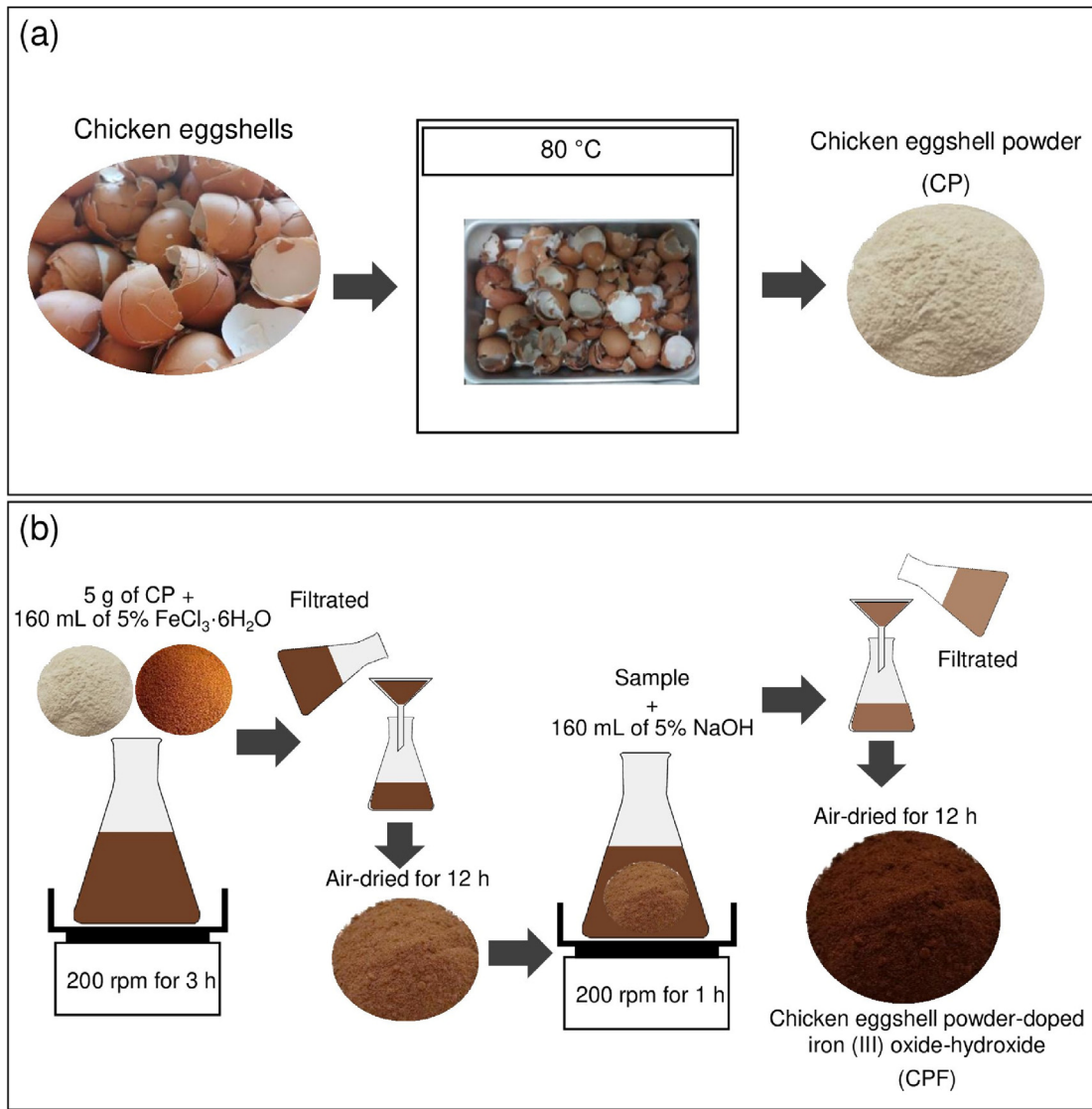


Fig. 1 Flow diagram of synthesis methods of (a) CP and (b) CPF.

efficiency, and that value was applied to the next affecting factor study. The atomic adsorption spectrophotometer (PerkinElmer, PinAAcle 900F, USA) is used for analyzing lead concentrations, and triplicate experiments were conducted to confirm the results. Lead removal in the percentage (%) is calculated by following Eq. (1)

$$\text{Lead removal efficiency (\%)} = \left(\frac{C_0 - C_e}{C_0} \right) \times 100 \quad (1)$$

where C_0 is the initial lead concentration (mg/L), and C_e is the equilibrium of lead concentration in the solution (mg/L).

2.7. Adsorption isotherms

Linear and nonlinear Langmuir, Freundlich, Temkin, and Dubinin-Radushkevich models represented the adsorption process of monolayer or multi-layer or heat or thermodynamic is used for identifying the adsorption pattern of chicken eggshell powder (CP) and chicken eggshell powder-doped iron (III)

oxide-hydroxide (CPF), and their adsorption isotherms are calculated by Eqs. (2)–(9) (Dubinin and Radushkevich, 1947; Freundlich, 1906; Langmuir, 1918; Temkin and Pyzhev, 1940):

Langmuir isotherm:

$$\text{Linear : } \frac{C_e}{q_e} = \frac{1}{q_m K_L} + \frac{C_e}{q_m} \quad (2)$$

$$\text{Nonlinear : } q_e = \frac{q_m K_L C_e}{1 + K_L C_e} \quad (3)$$

Freundlich isotherm:

$$\text{Linear : } \log q_e = \log K_F + \frac{1}{n} \log C_e \quad (4)$$

$$\text{Nonlinear : } q_e = K_F C_e^{1/n} \quad (5)$$

Temkin isotherm:

$$\text{Linear : } q_e = \frac{RT}{b_T} \ln A_T + \frac{RT}{b_T} \ln C_e \quad (6)$$

$$\text{Nonlinear : } q_e = \frac{RT}{b_T} \ln A_T C_e \quad (7)$$

Dubinin-Radushkevich isotherm:

$$\text{Linear : } \ln q_e = \ln q_m - K_{DR} \varepsilon^2 \quad (8)$$

$$\text{Nonlinear : } q_e = q_m \exp(-K_{DR} \varepsilon^2) \quad (9)$$

where C_e is the equilibrium of lead concentration (mg/L), q_e is the amount of adsorbed lead on CP or CPF (mg/g), q_m is indicated the maximum amount of lead adsorption on CP or CPF (mg/g), K_L is the adsorption constant (L/mg). K_F is the constant of adsorption capacity (mg/g)(L/mg)^{1/n}, and $1/n$ is the constant depicting the adsorption intensity. R is the universal gas constant (8.314 J/mol K), T is the absolute temperature (K), b_T is the constant related to the heat of adsorption (J/mol), and A_T is the equilibrium binding constant corresponding to the maximum binding energy (L/g). q_m is the theoretical saturation adsorption capacity (mg/g), K_{DR} is the activity coefficient related to mean adsorption energy (mol²/J²), and ε is the Polanyi potential (J/mol). Graphs of linear Langmuir, Freundlich, Temkin, and Dubinin-Radushkevich isotherms were plotted by C_e/q_e versus C_e , $\log q_e$ versus $\log C_e$, q_e versus $\ln C_e$, and $\ln q_e$ versus ε^2 , respectively whereas graphs of their nonlinear were plotted by q_e versus C_e .

For adsorption isotherm experiments, 0.5 g of CP or 0.3 g of CPF were added to 500 mL Erlenmeyer flasks with variable lead concentrations from 10 to 70 mg/L. The control condition of CP or CPF was a sample volume of 200 mL, a shaking speed of 200 rpm, pH 5, a temperature of 25 °C, and a contact time of 4 h for CP and 2 h for CPF.

2.8. Adsorption kinetics

Linear and nonlinear pseudo-first-order kinetic, pseudo-second-order kinetic, elovich, and intraparticle diffusion models are used for studying the adsorption mechanism of chicken eggshell powder (CP) and chicken eggshell powder-doped iron (III) oxide-hydroxide (CPF), and their adsorption kinetic equations are calculated by Eqs. (10)–(16) (Elovich and Larinov, 1962; Ho and McKay, 1999; Lagergren, 1898; Weber and Morris, 1963):

Pseudo-first-order kinetic model:

$$\text{Linear : } \ln (q_e - q_t) = \ln q_e - k_1 t \quad (10)$$

$$\text{Nonlinear : } q_t = q_e (1 - e^{-k_1 t}) \quad (11)$$

Pseudo-second-order kinetic model:

$$\text{Linear : } \frac{t}{q_t} = \frac{1}{k_2 q_e^2} + \left(\frac{1}{q_e} \right) t \quad (12)$$

$$\text{Nonlinear : } q_t = \frac{k_2 q_e^2 t}{1 + q_e k_2 t} \quad (13)$$

Elovich model:

$$\text{Linear : } q_t = \frac{1}{\beta} \ln (\alpha \beta) + \frac{1}{\beta} \ln t \quad (14)$$

$$\text{Nonlinear : } q_t = \beta \ln t + \beta \ln \alpha \quad (15)$$

Intra-particle diffusion model:

$$\text{Linear and nonlinear : } q_t = k_i t^{0.5} + C_i \quad (16)$$

where q_e is the amount of adsorbed lead on adsorbent materials (mg/g), q_t is the amount of adsorbed lead at the time (t) (mg/g), k_1 is a pseudo-first-order rate constant (min⁻¹), and k_2 is a pseudo-second-order rate constant (g/mg·min). α is the initial adsorption rate (mg/g/min) and β is the extent of surface coverage (g/mg). k_i is the intraparticle diffusion rate constant (mg/g·min^{0.5}) and C_i is the constant that gives an idea about the thickness of the boundary layer (mg/g). Graphs of linear pseudo-first-order, pseudo-second-order, elovich, and intraparticle diffusion models were plotted by $\ln (q_e - q_t)$ versus time (t), t/q_t versus time (t), q_t versus $\ln t$, and q_t versus time ($t^{0.5}$), respectively whereas their nonlinear graphs were plotted by the capacity of lead adsorbed by adsorbent materials at the time (q_t) versus time (t).

For adsorption kinetic experiments, 2.5 g of CP or 1.5 g of CPF were added to 1000 mL of breaker with the lead concentration of 50 mg/L. The control condition of CP and CPF was a sample volume of 1000 mL, a shaking speed of 200 rpm, pH 5, a temperature of 25 °C, and a contact time of 6 h.

2.9. Desorption experiments

The desorption experiments are designed to examine the possible material reusability by studying five adsorption–desorption cycles to confirm the abilities of chicken eggshell powder (CP) and chicken eggshell powder-doped iron (III) oxide-hydroxide (CPF) for lead adsorption. After an adsorption process, CP or CPF was added to 500 mL of Erlenmeyer flask containing 200 mL of 0.5 M HNO₃ solution, then it was shaken by an incubator shaker (New Brunswick, Innova 42, USA) at 200 rpm for 4 h. After that, it was washed with deionization water and dried at room temperature, and CP or CPF is ready for the next adsorption cycle. The desorption efficiency in percentage is calculated by following Eq (17):

$$\text{Desorption (\%)} = \left(\frac{q_d}{q_a} \right) \times 100 \quad (17)$$

where q_d is the amount of lead desorbed (mg/mL) and q_a is the amount of lead adsorbed (mg/mL).

3. Result and discussion

3.1. The physical characteristics of chicken eggshell powder (CP) and chicken eggshell powder-doped iron (III) oxide-hydroxide (CPF)

The physical characteristics of CP and CPF are demonstrated in Fig. 2a-b. CP was a cream color powder matching the color of a chicken eggshell shown in Fig. 2a while CPF was an iron-rust color powder corresponding to a color of iron (III) oxide-hydroxide color shown in Fig. 2b.

3.2. Characterizations of chicken eggshell powder (CP) and chicken eggshell powder-doped iron (III) oxide-hydroxide (CPF)

3.2.1. BET analysis

The specific surface area, pore volume, and pore diameter size of CP and CPF were determined by the Brunauer-Emmet and



Fig. 2 The physical characteristics of (a) CP and (b) CPF.

Teller technique (BET) with N_2 adsorption–desorption isotherm at 77.3 K and degas temperature of 80 °C for 6 h, and the results of Barrett-Joyner-Halenda (BJH) method reported in Table 2.

The specific surface area of CP and CPF were 0.692 and 17.382 m^2/g which CPF demonstrated a higher specific surface area than CP. The pore volumes of CP and CPF were 0.001 and 0.011 cm^3/g and their pore diameter sizes were 3.597 and 2.617 nm. As a result, CPF had a higher pore volume and a smaller pore diameter size than CP. The specific surface area and pore volume of CPF were higher than CP about 25 times and 11 times of CP which might be from the formation of iron (III) oxide-hydroxide in CPF. Therefore, the addition of iron (III) oxide-hydroxide into chicken eggshell powder increased the surface area and pore volume while the pore diameter size was decreased. Moreover, they were classified to be mesoporous materials since their pore diameter sizes were in a range of 2–50 nm following the classification by the International Union of Pure and Applied Chemistry (IUPAC) (Rouquerol et al., 1994).

3.2.2. XRD analysis

XRD patterns of CP and CPF by XRD analysis were demonstrated in Fig. 3a-b. For CP, it illustrated a semi-crystalline structure by presenting the specific calcium carbonate peaks of 23.16°, 29.53°, 30.65°, 36.08°, 39.51°, 43.26°, 47.63°, 48.61°, 57.43°, 60.70°, 64.68°, and 72.95° matched to JCPDS No. 05–0586 (Praipipat et al., 2022b). For CPF, it demonstrated a semi-crystalline structure by presenting the specific calcium carbonate peaks similarly to CP, and it also detected the specified iron (III) oxide-hydroxide peaks of 33.06°, 41.20°, and 53.68° following JCPDS No. 29–0713 (Huang et al., 2018). As a result, it could be confirmed by the successfully adding of iron (III) oxide-hydroxide to synthesize CPF.

Table 2 The specific surface area, pore volume, and pore size of CP and CPF.

Material	Specific surface area (m^2/g)	Pore volume (cm^3/g)	Pore diameter size (nm)
CP	0.692	0.001	3.597
CPF	17.382	0.011	2.617

3.2.3. FESEM-FIB and EDX analysis

The surface morphologies of CP and CPF by FESEM-FIB analysis at 2500X magnification with 50 μm illustrated in Fig. 4a-b. Both materials were irregular, rough, and uneven surfaces, so the addition of iron (III) oxide-hydroxide did not affect the surface morphology of CPF.

The chemical compositions of CP and CPF by EDX analysis are demonstrated in Fig. 4c-d. Three main chemical components of carbon (C), oxygen (O), and calcium (Ca) were found in both materials. CP and CPF contained 42.0 and 28.9 wt% O, 35.0 and 27.7 %wt Ca, 22.9 and 18.9 %wt C, 0 and 0.2 %wt Cl, and 0 and 24.3 %wt Fe, respectively. After adding iron (III) oxide-hydroxide, iron (Fe) was detected in CPF which confirmed the successful addition of iron (III) oxide-hydroxide. The addition of iron (III) oxide-hydroxide affected to the decreases of C, O, and Ca by increasing of Fe which might be from the formation of iron (III) oxide-hydroxide in CPF. Moreover, Na also detected in CPF might be from chemicals of ferric chloride hexahydrate ($FeCl_3 \cdot 6H_2O$) used for material synthesis.

3.2.4. FT-IR analysis

The chemical functional groups of CP and CPF were examined by FT-IR analysis, and their FT-IR spectra before and after lead adsorptions are demonstrated in Fig. 5a-b. Five main function groups of O–H, N–H, C=O, C–O, and C–H were detected in both materials, whereas Fe–O was only found in CPF which might be from the addition of iron (III) oxide-hydroxide. For O–H, it represented the stretching of the hydroxyl group and acidic hydrogen group, and N–H was the amine and amide presented in the protein fiber of the eggshell membrane (Lulit et al., 2019). C=O referred to the stretching of the amide and carbonyl group, and C–O was the stretching of the carbonate group presented calcium oxide (CaO) in eggshells (Awogbemi et al., 2020). In addition, C–H was the bending of calcium carbonate ($CaCO_3$) (Tizo et al., 2018).

For before lead adsorption, CP detected the stretching of O–H at 3350.05 cm^{-1} , N–H at 2327.00 cm^{-1} , stretching of C=O at 1796.26 and 1665.68 cm^{-1} , stretching of C–O at 1402.17 cm^{-1} , and bending of C–H at 872.22 and 711.78 cm^{-1} shown in Fig. 5a, and CPF detected the stretching of O–H at 3349.52 cm^{-1} , N–H at 2327.32 cm^{-1} , stretching of

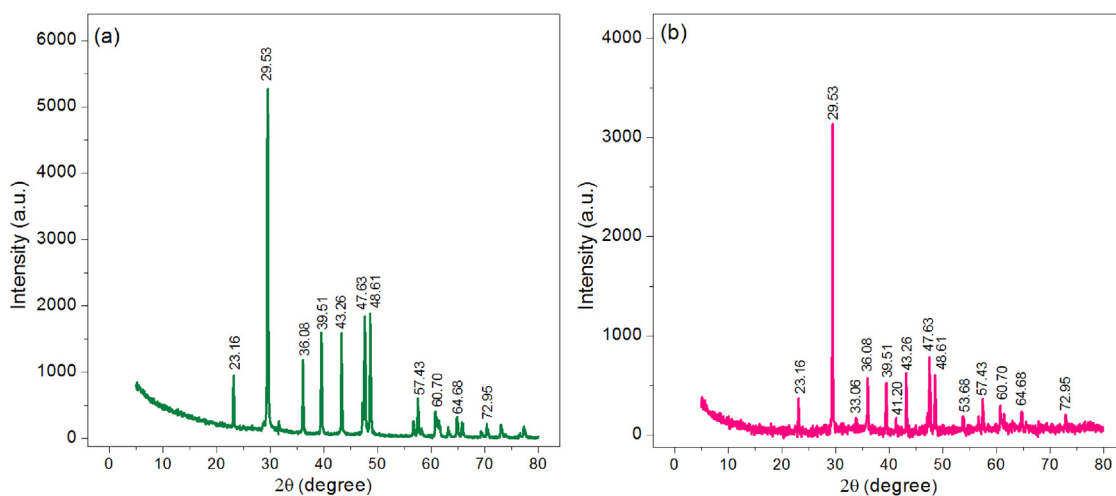


Fig. 3 XRD patterns of (a) CP and (b) CPF.

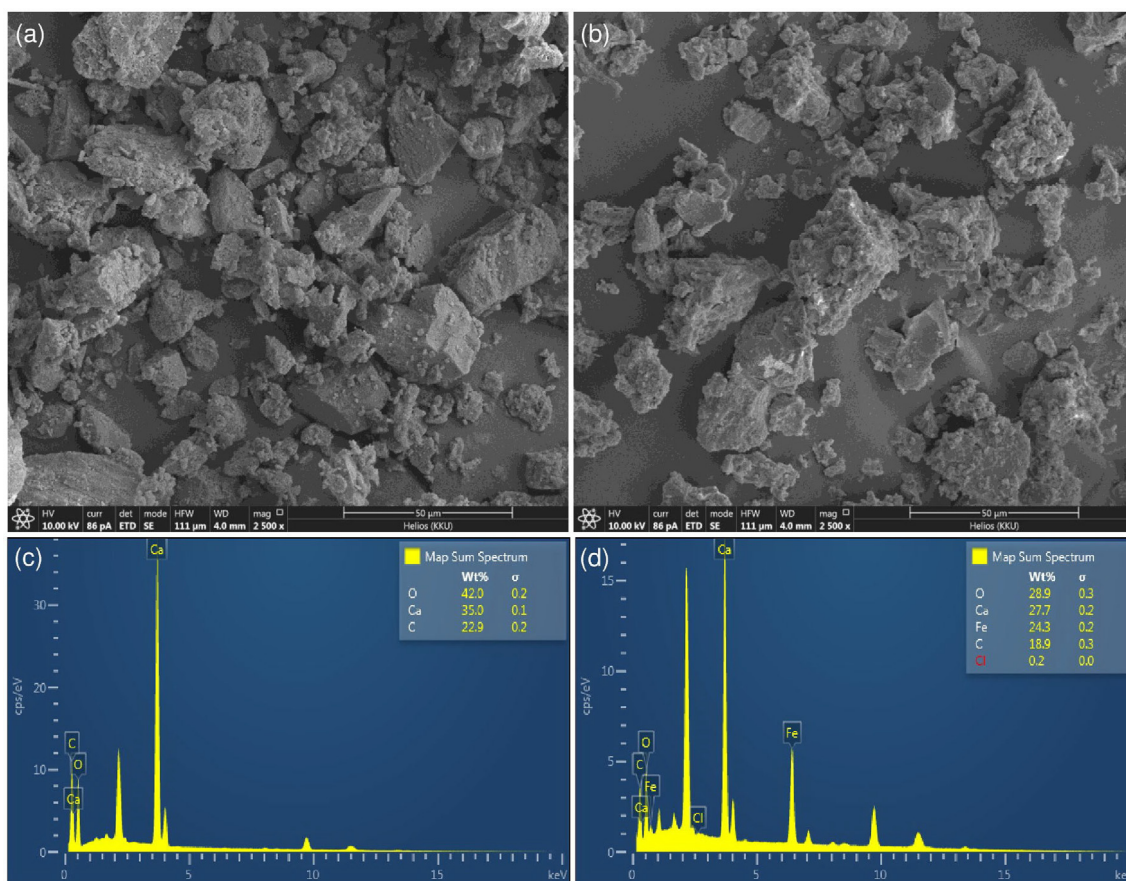


Fig. 4 The surface morphologies and chemical compositions of (a, c) CP and (b, d) CPF.

C=O at 1788.75 and 1665.52 cm^{-1} , stretching of C—O at 1407.37 cm^{-1} , bending of C—H at 871.98 and 710.68 cm^{-1} , and Fe—O was 630.28 cm^{-1} shown in Fig. 5b.

For after lead adsorption, CP detected the stretching of O—H at 3286.58 cm^{-1} , N—H at 2509.98 cm^{-1} , stretching of C=O at 1795.79 cm^{-1} , stretching of C—O at 1396.43 cm^{-1} ,

and bending of C—H at 871.45 and 711.38 cm^{-1} shown in Fig. 5a, and CPF detected the stretching of O—H at 3318.96 cm^{-1} , N—H at 2509.43 cm^{-1} , stretching of C=O at 1795.64 and 1639.95 cm^{-1} , stretching of C—O at 1406.51 cm^{-1} , bending of C—H at 871.97 and 710.26 cm^{-1} , and Fe—O was 625.49 cm^{-1} shown in Fig. 5b.

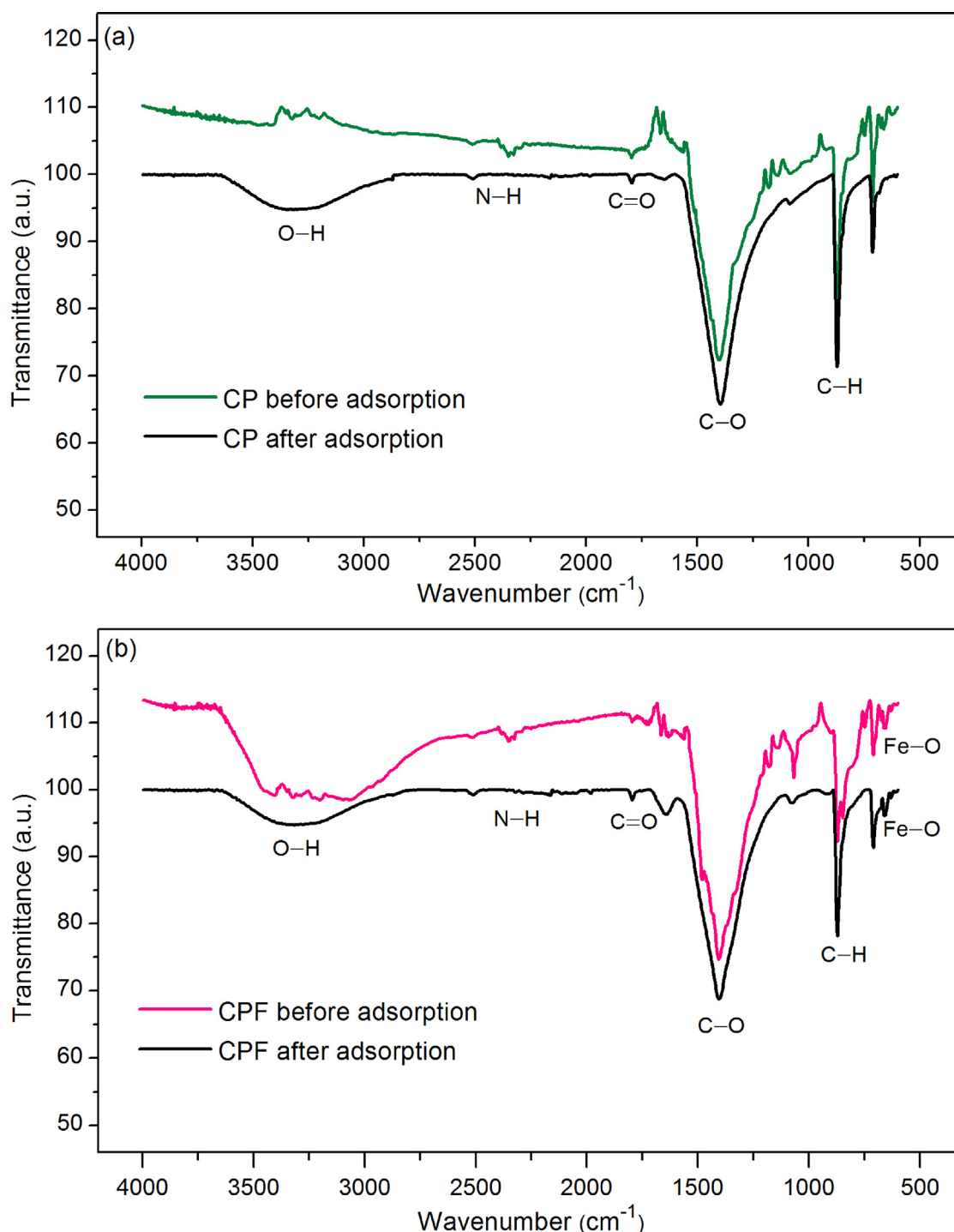


Fig. 5 The chemical functional groups before and after lead adsorptions of (a) CP and (b) CPF.

For comparing FT-IR spectra of before and after lead adsorption of CP and CPF, it observed the low frequency of bands of main functional groups after lead adsorption. In addition, the low intensity or shifting band was also observed which might be from adsorbing lead by CP and CPF. Especially, the bands around 3286.58 and 1396.43 cm^{-1} of CP and 3318.96 and 1406.51 cm^{-1} of CPF demonstrated the main observations for happening lead adsorption by O—H and C—O groups in CP and CPF by indicating Pb—O stretching for adsorbing lead by CP and CPF.

3.3. The point of zero charges of chicken eggshell powder (CP) and chicken eggshell powder-doped iron (III) oxide-hydroxide (CPF)

The point of zero charge (pH_{pzc}) is generally used for determining which pH value is good for lead adsorption by material. A pH value at the net charge equal to zero of the adsorbent is the pH_{pzc} of the material. The results of pH_{pzc} of CP and CPF are demonstrated in Fig. 6a-b. The pH_{pzc} values of CP and CPF were 4.47 and 4.83, so the addition of iron

(III) oxide-hydroxide affected the increase of pH_{pzc} . For lead adsorption, high lead adsorption should occur at the pH solution higher than the pH_{pzc} ($pH_{\text{solution}} > pH_{pzc}$) of the material because the surface of the material is negatively charged. Therefore, the high lead adsorption by CP and CPF should be found at a pH solution higher than the pH of 4 ($pH_{\text{solution}} > 4$) similarly reported by other studies (Ngamsurach et al., 2022a; Praipipat et al., 2023a; Threpanich and Praipipat, 2021, 2022).

3.4. Batch adsorption experiments

3.4.1. The effect of dose

The effect of dose was investigated lead removal efficiencies by varying six different dosages from 0.1 to 0.6 g of chicken eggshell powder (CP) and chicken eggshell powder-doped iron (III) oxide-hydroxide (CPF) with the control condition of the lead concentration of 50 mg/L, a sample volume of 200 mL, a contact time of 4 h, pH 5, a temperature of 25 °C, and a shaking speed of 200 rpm, and the results are demonstrated in Fig. 7a. Lead removal efficiencies of both materials were increased with the increase in dosage which might be from the increase of surface area or active sites of materials for adsorbing lead (Ngamsurach et al., 2022a). Their highest lead removal efficiencies were 95.89 % at 0.5 g for CP and 100 % at 0.3 g for CPF. Therefore, they were optimum doses of CP and CPF that were used for studying the contact time effect.

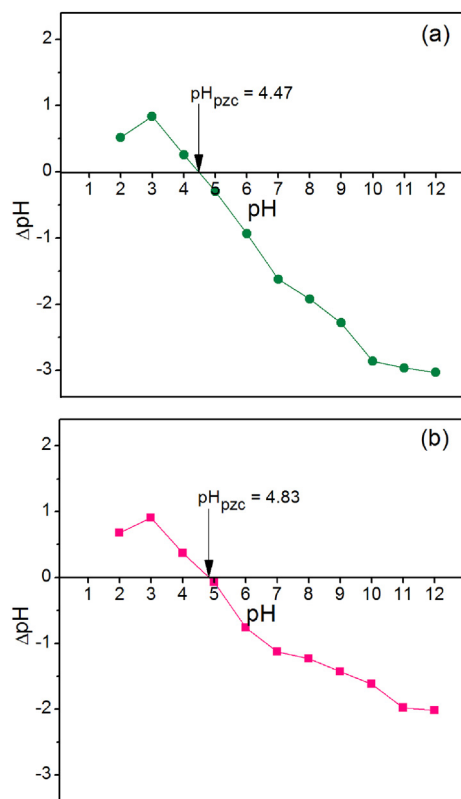


Fig. 6 The point of zero charges of (a) CP and (b) CPF.

3.4.2. The effect of contact time

The effect of contact time was investigated lead removal efficiencies by varying six different contact times from 1 to 6 h of CP and CPF with the control condition of the lead concentration of 50 mg/L, a sample volume of 200 mL, pH 5, a temperature of 25 °C, a shaking speed of 200 rpm, and the optimum dose from 3.4.1, and the results are demonstrated in Fig. 7b. Lead removal efficiencies of both materials were increased with the increase of contact time similar to the dose effect, and the saturated lead adsorption on the material is generally found at the highest lead removal efficiency. Their highest lead removal efficiencies were 94.36 % at 4 h for CP and 100 % at 2 h for CPF. Therefore, they were the optimum contact time of CP and CPF which were used for studying the pH effect.

3.4.3. The effect of pH

The effect of pH was investigated lead removal efficiencies by varying six different pH from 1 to 11 as respective pH conditions of acid, neutral, and alkaline of CP and CPF with the control condition of the lead concentration of 50 mg/L, a sample volume of 200 mL, a temperature of 25 °C, a shaking speed of 200 rpm, and the optimum dose and contact time from 3.4.1 and 3.4.2, and the results are demonstrated in Fig. 7c. Lead removal efficiencies of both materials were increased with the increase of pH values from 1 to 5, then they were decreased. Their highest lead removal efficiencies were found at pH 5 with lead removal at 95.27 % and 99.23 % for CP and CPF. This result corresponded to the result of pH_{pzc} of CP and CPF and other previous studies that reported the highest lead removal efficiency at $pH > 4$ (Ngamsurach et al., 2022a; Threpanich and Praipipat, 2022, 2021). Therefore, pH 5 was the optimum pH of CP and CPF which were used for studying the concentration effect.

3.4.4. The effect of concentration

The effect of concentration was investigated lead removal efficiencies by varying seven different concentrations from 10 to 70 mg/L of CP and CPF with the control condition of a sample volume of 200 mL, a temperature of 25 °C, a shaking speed of 200 rpm, and the optimum dose, contact time, and pH from 3.4.1, 3.4.2, and 3.4.3, and the results are demonstrated in Fig. 7d. Lead removal efficiencies of CP were 100 % from 10 to 30 mg/L after they were decreased to 90.90 % at 70 mg/L whereas lead removal efficiencies of CPF were 100 % from 10 to 40 mg/L after they were decreased to 93.74 % at 70 mg/L. The decreasing of lead removal efficiencies of both materials from the increasing of lead concentrations might be from the active sites of them did not enough to caught up with lead ions similarly reported by other studies (Ngamsurach et al., 2022a; Threpanich and Praipipat, 2022, 2021). For the lead concentration of 50 mg/L, lead removal efficiencies of CP and CPF were 95.35 % and 99.57 %, and CPF demonstrated a higher lead removal efficiency than CP.

In conclusion, 0.5 g, 4 h, pH 5, 50 mg/L and 0.3 g, 2 h, pH 5, 50 mg/L were the optimum conditions in dose, contact time, pH, and concentration of CP and CPF for lead removal efficiencies of 95.35 % and 99.57 %, respectively. Since CPF spent less material dosage and contact time than CP with having a higher lead removal efficiency than CP, so the addition of iron (III) oxide-hydroxide helped to improve material efficiency for

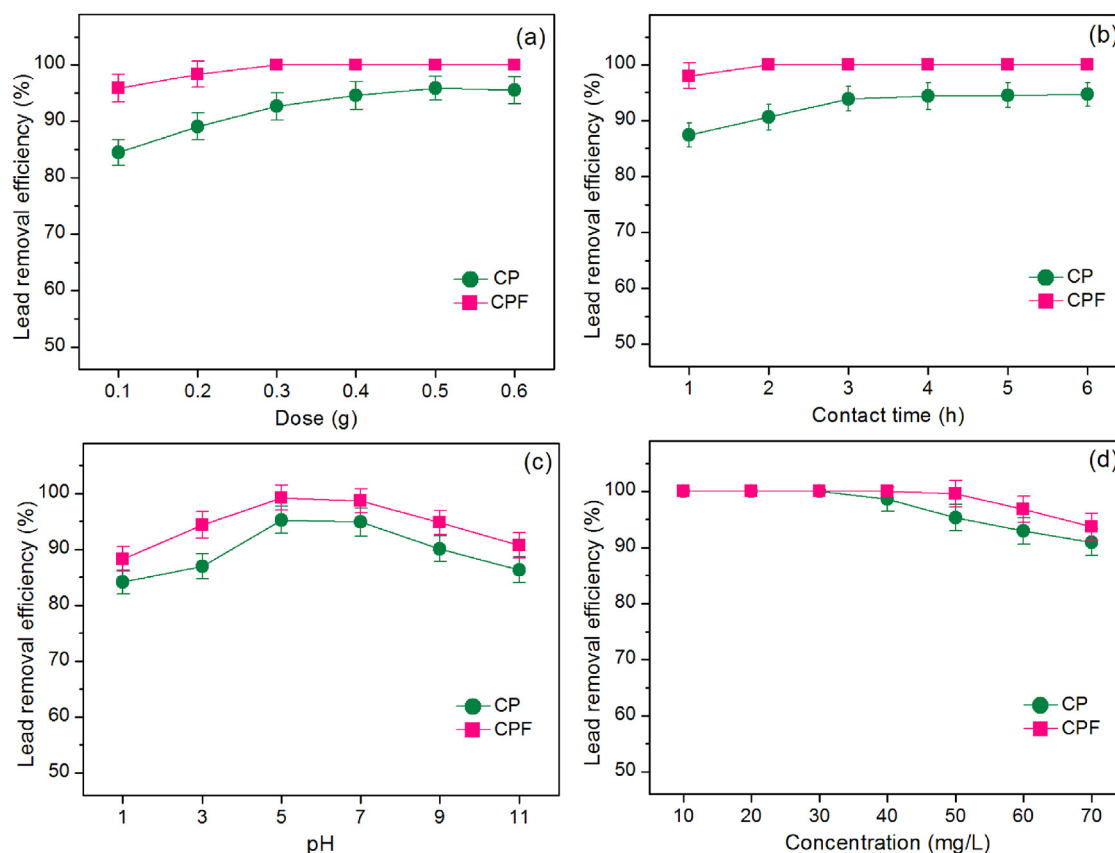


Fig. 7 Batch experiments on the effects of (a) dose, (b) contact time, (c) pH, and (d) concentration of CP and CPF for lead adsorptions.

lead adsorption similar reported by previous studies (Threepanich and Praipipat, 2021). CPF was recommended to be applied for lead removal in future industrial applications.

3.5. Adsorption isotherms

Linear and nonlinear models of Langmuir, Freundlich, Temkin, and Dubinin-Radushkevich models were used for investigating the adsorption patterns of chicken eggshell powder (CP) and chicken eggshell powder-doped iron (III) oxide-hydroxide (CPF) for lead adsorptions. For linear models, Langmuir, Freundlich, Temkin, and Dubinin-Radushkevich isotherms were plotted by C_e/q_e versus C_e , $\log q_e$ versus $\log C_e$, q_e versus $\ln C_e$, and $\ln q_e$ versus e^2 , respectively. For nonlinear models, all isotherms were plotted by C_e versus q_e . The plotting graph results are demonstrated in Fig. 8-a-f, and the equilibrium isotherm parameters are illustrated in Table 3.

For linear models, the Langmuir maximum adsorption capacities (q_m) of CP and CPF were 25.189 and 42.735 mg/g, and Langmuir adsorption constants (K_L) of CP and CPF were 4.315 and 7.548 L/mg. For Freundlich isotherm, the $1/n$ values of CP and CPF were 0.258 and 0.172. Freundlich adsorption constants (K_F) of CP and CPF were 16.776 and 31.893 (mg/g)(L/mg) $^{1/n}$. For Temkin isotherm, b_T values of CP and CPF were 796.126 and 749.817 J/mol, and A_T values of CP and CPF were 349.521 and 20859.232 L/g. For the Dubinin-Radushkevich model, the maximum adsorption capacities (q_m) of CP and CPF were 20.075 and 30.631 mg/g, and the

activity coefficient (K_{DR}) values of CP and CPF were 0.013 and 0.003 mol 2 /J 2 . The adsorption energy (E) values of CP and CPF were 6.299 and 12.500 kJ/mol. R^2 values of CP and CPF on Langmuir and Freundlich models were 0.993, 0.991 and 0.942, 0.993, respectively. In addition, R^2 values of CP and CPF on Temkin and Dubinin-Radushkevich models were 0.988, 0.904 and 0.941, 0.841, respectively.

For nonlinear models, the Langmuir maximum adsorption capacities (q_m) of CP and CPF were 25.493 and 40.762 mg/g, and Langmuir adsorption constants (K_L) of CP and CPF were 4.822 and 7.212 L/mg. For Freundlich isotherm, the $1/n$ values of CP and CPF were 0.215 and 0.181. Freundlich adsorption constants (K_F) of CP and CPF were 16.842 and 32.109 (mg/g)(L/mg) $^{1/n}$. For Temkin isotherm, b_T values of CP and CPF were 805.753 and 751.870 J/mol, and A_T values of CP and CPF were 346.447 and 20865.050 L/g. For the Dubinin-Radushkevich model, the maximum adsorption capacities (q_m) of CP and CPF were 20.218 and 31.766 mg/g, and the activity coefficient (K_{DR}) values of CP and CPF were 0.015 and 0.006 mol 2 /J 2 . The adsorption energy (E) values of CP and CPF were 5.695 and 9.178 kJ/mol. R^2 values of CP and CPF on Langmuir and Freundlich models were 0.994, 0.993 and 0.948, 0.995, respectively. In addition, R^2 values of CP and CPF on Temkin and Dubinin-Radushkevich models were 0.989, 0.907 and 0.942, 0.844, respectively. Moreover, R_{adj}^2 of CP and CPF in nonlinear Langmuir and Freundlich models were 0.993, 0.991 and 0.937, 0.994, respectively. R_{adj}^2 of CP and CPF in nonlinear Temkin and Dubinin-Radushkevich models were 0.987, 0.889 and 0.931, 0.812, respectively.

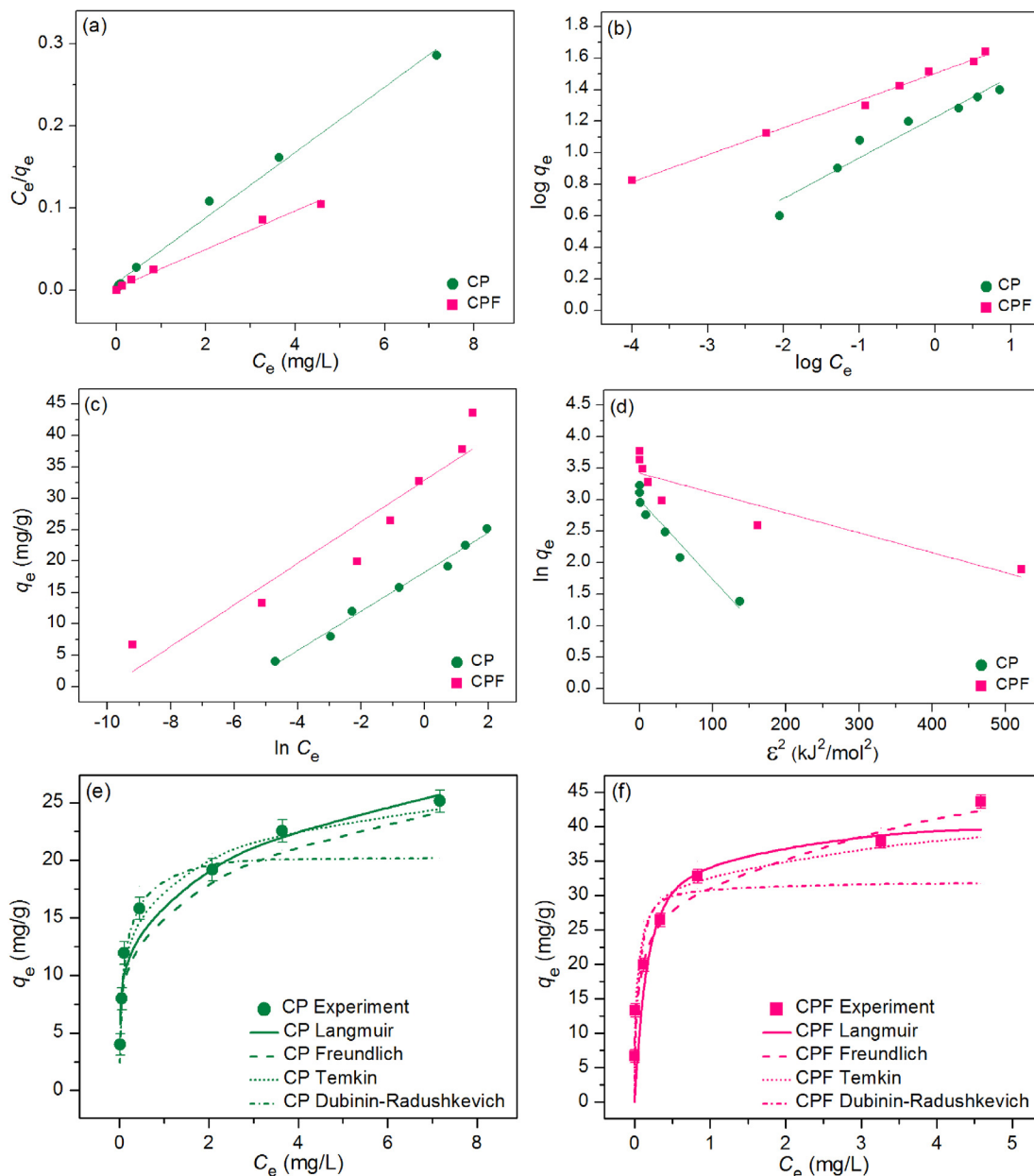


Fig. 8 Graphs of (a) linear Langmuir, (b) linear Freundlich, (c) linear Temkin, (d) linear Dubinin- Radushkevich, and (e) nonlinear adsorption isotherms of CP and (f) CPF for lead adsorptions.

For R^2 value consideration, since R^2 values of CP in both linear and nonlinear Langmuir models were higher than Freundlich, Temkin, and Dubinin-Radushkevich models, its adsorption patterns corresponded to Langmuir isotherm relating to physical adsorption. On the other hand, since R^2 values of CPF in both linear and nonlinear Freundlich models were higher than Langmuir, Temkin, and Dubinin-Radushkevich models, its adsorption patterns corresponded to Freundlich isotherm relating to physiochemical adsorption. For the Langmuir model, the parameters of q_m and K_L were used for explaining the adsorption pattern. Since CPF had higher q_m and K_L values in both linear and nonlinear models than CP, CPF could remove lead with a faster adsorption rate than CP. For the Freundlich model, K_F and $1/n$ values were used

for consideration. Normally, if the $1/n$ value is in a range of 0–1 that means the adsorbent is favorable adsorption (Eltaweil et al., 2022). Since $1/n$ values in both linear and nonlinear models of CP and CPF were in a range of $0 > 1/n > 1$, both materials were favorable lead adsorption. In addition, the K_F values in both linear and nonlinear models of CPF had higher than CP, so CPF could adsorb lead with a faster adsorption rate than CP. For the Temkin model, the A_T is generally used for consideration in which a high A_T demonstrates stronger energy for equilibrium adsorption of adsorbent. CPF illustrated a higher A_T value in both linear and nonlinear models than CP, so CPF had stronger energy for equilibrium lead adsorption than CP. For the Dubinin-Radushkevich model, the parameters of q_m and E are normally used for explaining

Table 3 The comparison of linear and nonlinear isotherm parameters for lead adsorptions on CP and CPF.

Regression methods	Isotherm models	Parameters	CP	CPF	
Linear	Langmuir	q_m (mg/g)	25.189	42.735	
		K_L (L/mg)	4.315	7.548	
		R^2	0.993	0.991	
	Freundlich	$1/n$	0.258	0.172	
		K_F (mg/g)(L/mg) ^{1/n}	16.776	31.893	
		R^2	0.942	0.993	
	Temkin	b_T (J/mol)	796.126	749.817	
		A_T (L/g)	349.521	20859.232	
		R^2	0.988	0.904	
	Dubinin-Radushkevich	q_m (mg/g)	20.075	30.631	
		K_{DR} (mol ² /J ²)	0.013	0.003	
		E (kJ/mol)	6.299	12.500	
		R^2	0.941	0.841	
	Nonlinear	Langmuir	q_m (mg/g)	25.493	40.762
			K_L (L/mg)	4.822	7.212
			R^2	0.994	0.993
R^2_{adj}			0.993	0.991	
RMSE			3.185	6.526	
$1/n$			0.215	0.181	
Freundlich		K_F (mg/g)(L/mg) ^{1/n}	16.842	32.109	
		R^2	0.948	0.995	
		R^2_{adj}	0.937	0.994	
		RMSE	1.937	1.611	
		b_T (J/mol)	805.753	751.870	
		A_T (L/g)	346.447	20865.050	
Temkin		R^2	0.989	0.907	
		R^2_{adj}	0.987	0.889	
		RMSE	1.055	6.684	
		q_m (mg/g)	20.218	31.766	
		K_{DR} (mol ² /J ²)	0.015	0.006	
		E (kJ/mol)	5.695	9.178	
Dubinin-Radushkevich		R^2	0.942	0.844	
		R^2_{adj}	0.931	0.812	
		RMSE	2.736	7.267	

the adsorption pattern. For the q_m value, it corresponded to the q_m of the Langmuir model that a higher q_m value demonstrated a higher adsorption capacity of the adsorbent. For the E value, if the E value is lower than 8 kJ/mol represented the physisorption process, whereas if the E value is in a range of 8–16 kJ/mol represented the chemisorption process. As a result, the adsorption pattern of CP was physisorption with the E value of 5.695 and 6.299 kJ/mol in linear and nonlinear models corresponding to the Langmuir model which was the best fitted model of CP. Oppositely, the adsorption pattern of CPF was chemisorption with the E value of 12.500 and 9.178 kJ/mol in linear and nonlinear models corresponding to the Freundlich model which was the best fitted model of CPF. Moreover, both linear and nonlinear isotherm models were recommended to plot graphs for confirming the results and protecting against data mistranslation (Ngamsurach et al., 2022b; Ngamsurach and Praipipat, 2022a, 2022b, 2021).

Moreover, the comparison of the maximum adsorption capacity (q_m) value of eggshell adsorbents with and without modifications for lead adsorption is illustrated in Table 4. For unmodified comparison, CP and CPF had higher q_m values than previous studies (Alamillo-López et al., 2020; Hassan et al., 2020; Soares et al., 2016). For modified compar-

ison, both materials had also higher q_m values than the eggshell with acidic modification (Maxwell et al., 2020). In addition, their q_m values had higher than the eggshell with thermal treatment or calcination process except in the study of Gurav, V. L and Samant, R. A. which CP had a lower q_m value than this study. Moreover, CPF had a higher q_m value than the eggshells modified with Ag-Fe (Alamillo-López et al., 2020), so the addition of iron (III) oxide-hydroxide into the chicken eggshell of this study demonstrated a high material performance for lead adsorption in aqueous solution.

3.6. Adsorption kinetics

Linear and nonlinear kinetic models of pseudo-first-order kinetic model, pseudo-second-order kinetic model, elovich model, and intraparticle diffusion were used to determine the adsorption mechanism and rate of reaction of lead adsorptions by chicken eggshell powder (CP) and chicken eggshell powdered iron (III) oxide-hydroxide (CPF). For linear models, they were plotted by $\ln(q_e - q_t)$ versus time (t), t/q_t versus time (t), q_t versus $\ln t$, and q_t versus time ($t^{0.5}$) for pseudo-first-order kinetic, pseudo-second-order kinetic, elovich, and intraparticle diffusion models, respectively. For nonlinear models,

Table 4 Comparison of the maximum adsorption capacity (q_m) of various eggshell adsorbents for lead adsorption.

Materials	q_m (mg/g)	References
Eggshell	3.90	(Alamillo-López et al., 2020)
Eggshell	15.91	(Soares et al., 2016)
Eggshell	18.80	(Hassan et al., 2020)
Eggshell modified with HCl	16.95	(Maxwell et al., 2020)
Calcinated hen eggshell with silica gel	0.87	(Bayu et al., 2022)
Calcinated eggshell	29.60	(Gurav and Samant, 2021)
Calcium oxide from hen eggshell	0.88	(Kasirajan et al., 2022)
Eggshell modified with Ag-Fe	27.80	(Alamillo-López et al., 2020)
CP	25.19	This study
CPF	42.74	This study

they were plotted by q_t versus time (t). The plotting graph results are illustrated in Fig. 9a-f, and the adsorption kinetic parameters are presented in Table 5.

For linear models, the adsorption capacities (q_e) of CP and CPF on a pseudo-first-order kinetic model were 7.081 and 8.344 mg/g, and their reaction rate constants (k_1) were 0.014 and 0.013 min^{-1} . For a pseudo-second-order kinetic model, the adsorption capacities (q_e) of CP and CPF were 20.121 and 33.557 mg/g, and their reaction of rate constants (k_2) were 0.003 and 0.004 g/mg-min. For the elovich model, the initial adsorption rates (α) of CP and CPF were 0.901 and 0.719 mg/g/min, and their extents of surface coverage (β) were 0.286 and 0.179 g/mg. For the intraparticle diffusion model, the reaction of rate constants (k_i) of CP and CPF were 0.814 and 1.268 $\text{mg/g}\cdot\text{min}^{0.5}$, and their constant C_i values were 7.179 and 14.304 mg/g. R^2 values of CP and CPF on pseudo-first-order and pseudo-second-order kinetic models were 0.893, 0.818 and 0.996, 0.999, respectively. In addition, R^2 values of CP and CPF on elovich and intraparticle diffusion models were 0.894, 0.923 and 0.651, 0.638, respectively.

For nonlinear models, the adsorption capacities (q_e) of CP and CPF on a pseudo-first-order kinetic model were 7.640 and 8.503 mg/g, and their reaction rate constant (k_1) were 0.020 and 0.019 min^{-1} . For a pseudo-second-order kinetic model, the adsorption capacities (q_e) of CP and CPF were 21.023 and 34.916 mg/g, and their reaction of rate constants (k_2) were 0.002 and 0.002 g/mg-min. For the elovich model, the initial adsorption rates (α) of CP and CPF were 0.916 and 0.722 mg/g/min, and their extents of surface coverage (β) were 0.291 and 0.187 g/mg. For the intraparticle diffusion model, the reaction of rate constants (k_i) of CP and CPF were 0.825 and 1.376 $\text{mg/g}\cdot\text{min}^{0.5}$, and their constant C_i values were 7.334 and 14.683 mg/g. R^2 values of CP and CPF on pseudo-first-order and pseudo-second-order kinetic models were 0.892, 0.822 and 0.997, 0.998, respectively. In addition, R^2 values of CP and CPF on elovich and intraparticle diffusion models were 0.895, 0.928 and 0.656, 0.641, respectively. Moreover, R_{adj}^2 values of CP and CPF in nonlinear pseudo-first-order and pseudo-second-order kinetic models were 0.886, 0.811 and 0.996, 0.997, respectively. R_{adj}^2 values of CP and CPF in nonlinear elovich and intraparticle diffusion models were 0.889, 0.923 and 0.636, 0.620, respectively.

For R^2 value consideration, since R^2 values of CP and CPF in both linear and nonlinear pseudo-second-order kinetic models were higher than pseudo-first-order kinetic, elovich, and intraparticle diffusion models, so their adsorption rate and

mechanism of both materials corresponded to pseudo-second-order kinetic model with relating to a chemisorption process with heterogeneous adsorption. Therefore, the parameters of q_e and k_2 were used to describe the adsorption rate and mechanism. Since CPF demonstrated higher q_e values in both linear and nonlinear models than CP, CPF might adsorb lead higher than CP corresponding to batch experiments. In addition, the k_2 value of CPF was also higher values in both linear and nonlinear models than CP, so CPF demonstrated a faster reaction rate for lead adsorption than CP. For a pseudo-first-order kinetic model, the q_e and k_1 values of CPF in both linear and nonlinear models had also higher than CP similar to a pseudo-second-order kinetic model. For elovich, the parameters of α and β were used for consideration. Normally, if an α value is higher than a β value, the adsorption rate is higher than the desorption rate (Basha et al., 2022). In this study, both α values of CP and CPF had higher than β values in both linear and nonlinear models. For intraparticle diffusion, the C_i value is generally used for determining the type of adsorption mechanism of the adsorbent. If the C_i value is higher than zero ($C_i > 0$) that means the adsorption kinetic of the adsorbent is multiple steps of the intraparticle diffusion. Oppositely, if the C_i value is equal to zero ($C_i = 0$) that means the adsorption kinetic of the adsorbent is the sole rate-limiting step of the intraparticle diffusion (Basha et al., 2022). Since C_i values of CP and CPF in both linear and nonlinear models were higher than zero, they had multiple steps of intraparticle diffusion for lead adsorption. Finally, the graph plotting of both linear and nonlinear kinetic models was also recommended for correct data translations (Ngamsurach et al., 2022b; Ngamsurach and Praipipat, 2022a, 2022b, 2021).

3.7. Desorption experiments

The desorption experiments were used for investigating the feasibility for reuse materials because this is a necessary point to estimate the cost and economic feasibility of industrial applications. Lead adsorption tests of chicken eggshell powder (CP) and chicken eggshell powder-doped iron (III) oxide-hydroxide (CPF) for 5 cycles of adsorption-desorption were applied to confirm their abilities, and their results are illustrated in Fig. 10a-b. In Fig. 10a, CP could be reused in 5 cycles with high adsorption and desorption in ranges of 77.60–95.27 % and 70.28–94.92 %, respectively which adsorption and desorption were decreased by approximately 18 % and 25 %, respectively. For CPF, it also confirmed to be reusability

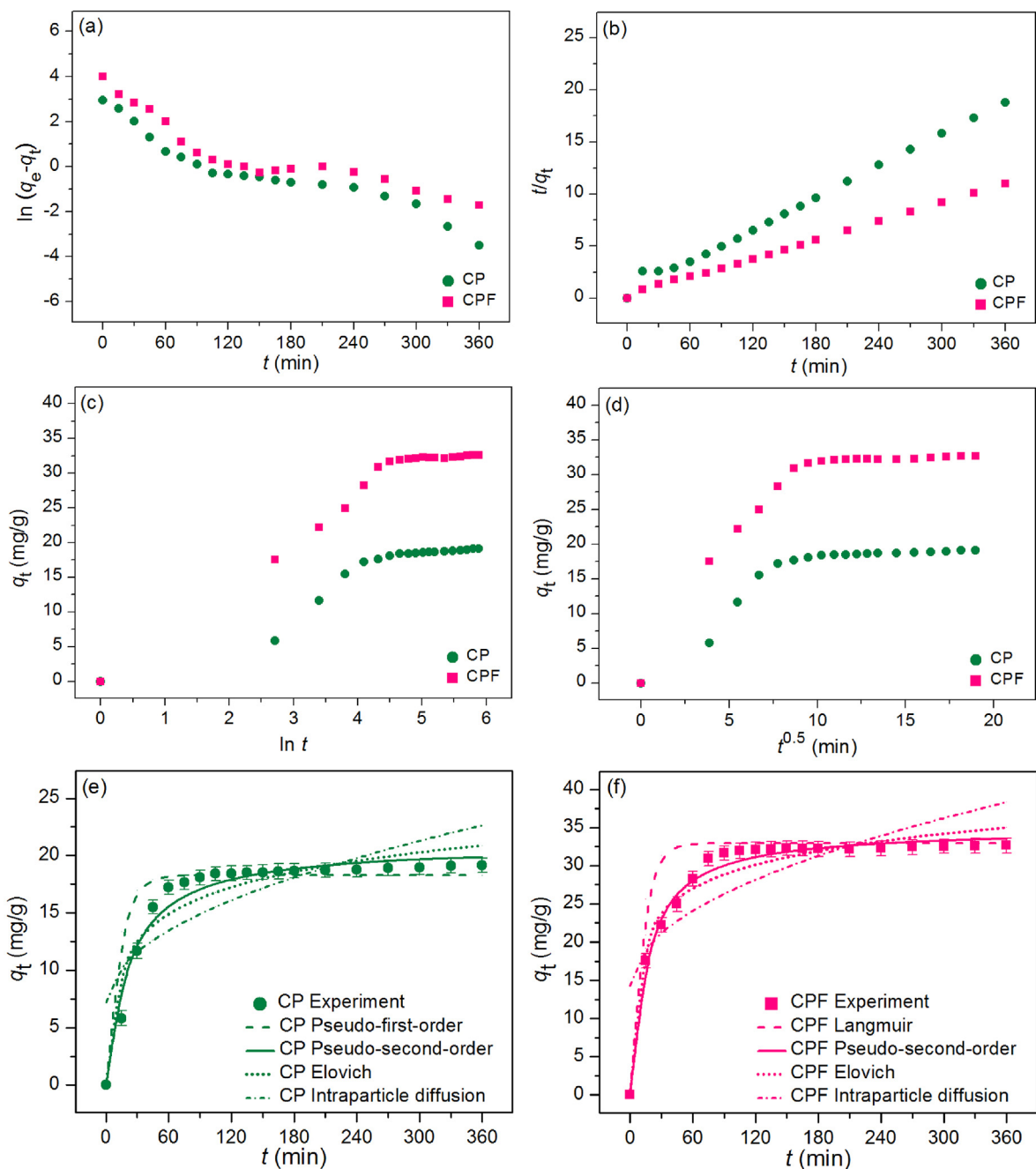


Fig. 9 Graphs of (a) linear pseudo-first-order, (b) linear pseudo-second-order, (c) linear elovich model (d) linear intraparticle diffusion, and (e) nonlinear kinetic models of CP and (f) CPF for lead adsorptions.

in 5 cycles with high adsorption and desorption in ranges of 84.52–99.49 % and 80.07–99.05 %, respectively which adsorption and desorption were decreased by approximately 15 % and 19 %, respectively shown in Fig. 10b. Therefore, both materials are potential materials for lead adsorption with the reusability of more than 5 cycles by more than 77 %, and they can be further applied to industrial applications.

4. The possible mechanisms of lead adsorption by chicken eggshell powder (CP) and chicken eggshell powder-doped iron (III) oxide-hydroxide (CPF)

The possible mechanisms of lead adsorption on CP and CPF was explained in Fig. 11a-b. The main structure of CP and CPF is composed of calcium carbonate (CaCO_3) with a hydro-

Table 5 The comparison of linear and nonlinear kinetic parameters for lead adsorptions on CP and CPF.

Regression methods	Kinetic models	Parameters	CP	CPF
Linear	Pseudo-first-order kinetic	q_e (mg/g)	7.081	8.344
		k_1 (min^{-1})	0.014	0.013
		R^2	0.893	0.818
	Pseudo-second-order kinetic	q_e (mg/g)	20.121	33.557
		k_2 (g/mg.min)	0.003	0.004
		R^2	0.996	0.999
	Elovich	α (mg/g.min)	0.901	0.719
		β (g/mg)	0.286	0.179
		R^2	0.894	0.923
	Intraparticle diffusion	k_i (mg/g.min ^{0.5})	0.814	1.268
		C_i (mg/g)	7.179	14.304
		R^2	0.651	0.638
Nonlinear	Pseudo-first-order kinetic	q_e (mg/g)	7.640	8.503
		k_1 (min^{-1})	0.020	0.019
		R^2	0.892	0.822
		R_{adj}^2	0.886	0.811
		RMSE	2.369	3.769
	Pseudo-second-order kinetic	q_e (mg/g)	21.023	34.916
		k_2 (g/mg.min)	0.002	0.002
		R^2	0.997	0.998
		R_{adj}^2	0.996	0.997
		RMSE	1.064	0.955
	Elovich	α (mg/g.min)	0.916	0.722
		β (g/mg)	0.291	0.187
		R^2	0.895	0.928
		R_{adj}^2	0.889	0.923
		RMSE	1.715	3.709
	Intraparticle diffusion	k_i (mg/g.min ^{0.5})	0.825	1.376
		C_i (mg/g)	7.334	14.683
		R^2	0.656	0.641
		R_{adj}^2	0.636	0.620
		RMSE	3.125	5.003

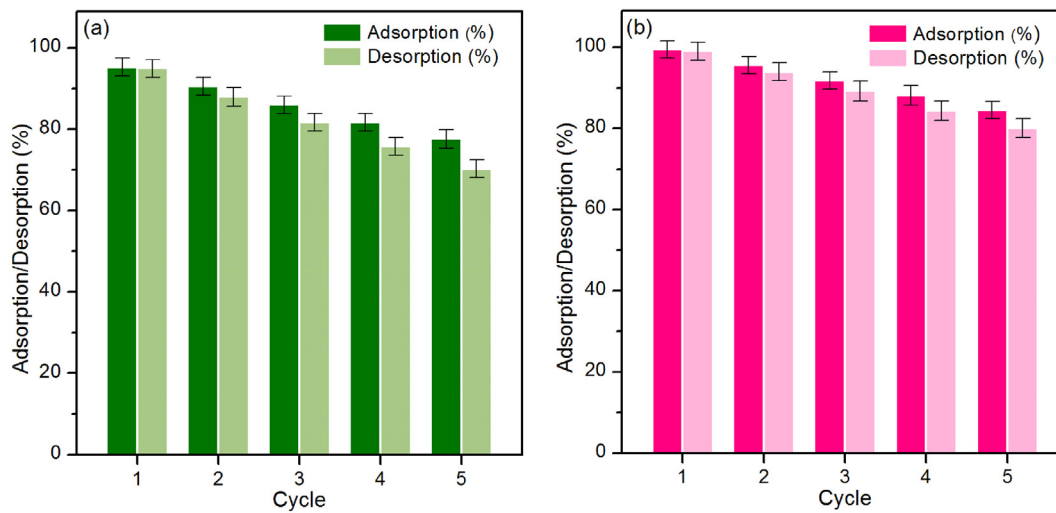


Fig. 10 The desorption experiments of (a) CP and (b) CPF.

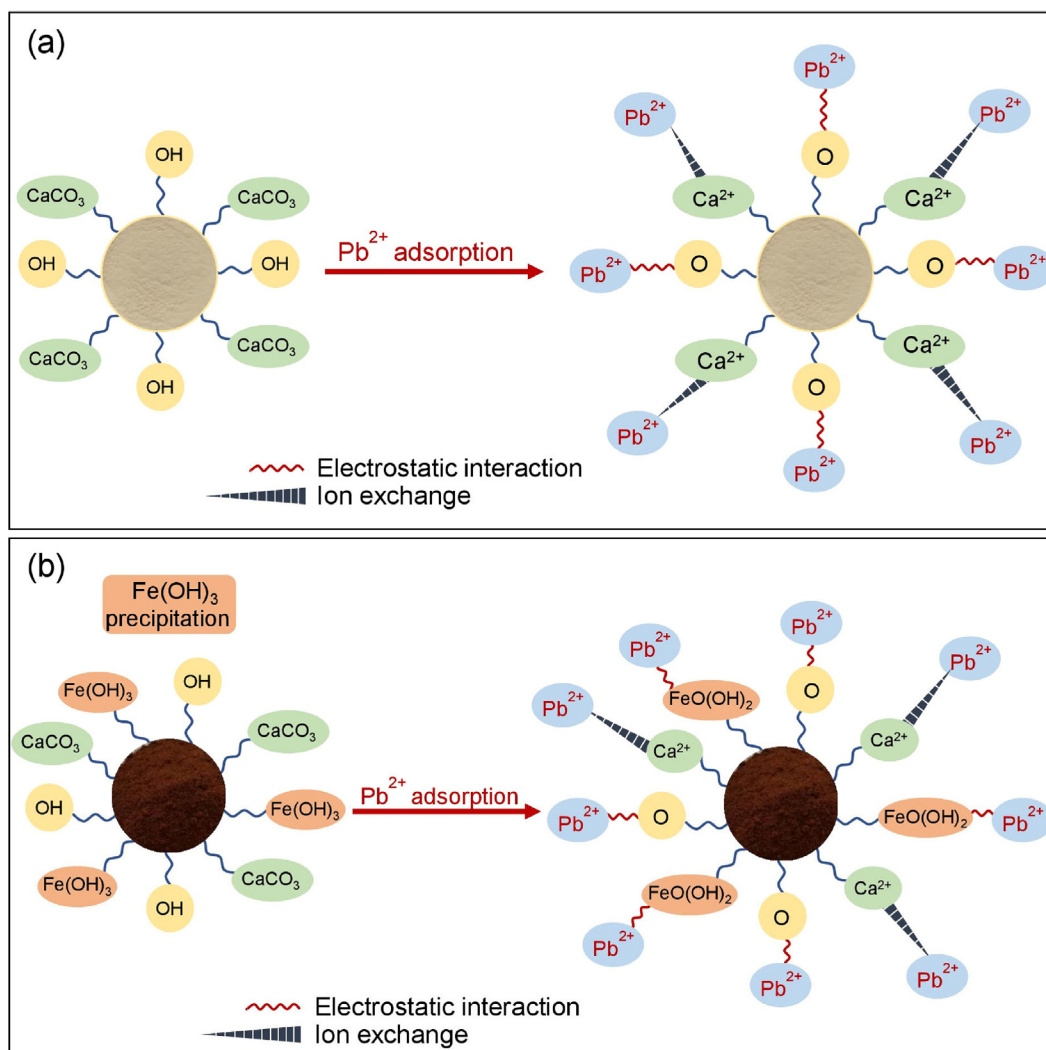


Fig. 11 Possible mechanisms of lead adsorption on (a) CP and (b) CPF.

xyl group ($-OH$) while CPF had also the complex compound of iron (III) oxide-hydroxide $CP \cdot Fe(OH)_3$ precipitation on its surface from adding iron (III) oxide-hydroxide into CP by sharing electrons with $-OH$ of CP. The possible mechanism of lead adsorptions by CP and CPF might occur from donating a proton (H^+) from $-OH$ or $CP \cdot Fe(OH)_3$ of the main chemical compounds for capturing lead (II) ions (Pb^{2+}) instead of H^+ from a process of electrostatic interaction (Wang et al., 2022). Moreover, the ion exchange from donating calcium ions (Ca^{2+}) from $CaCO_3$ for exchanging Ca^{2+} with Pb^{2+} on the surface of CP or CPF might possibly occur (Ahmad et al., 2012).

5. Conclusion

Chicken eggshell powder (CP) and chicken eggshell powder-doped iron (III) oxide-hydroxide (CPF) were successfully synthesized. The specific surface area and pore volume of CPF were higher than CP whereas its pore diameter size was smaller than CP. The crystalline structures of both materials illustrated semi-crystalline phases with presenting peaks of calcium carbonate. Their surface morphologies were irregular, rough, and uneven surfaces, and three main chemical elements of

carbon (C), calcium (Ca), and oxygen (O) were detected in both materials. Iron (Fe) was only found in CPF which could confirm the addition of iron (III) oxide-hydroxide into CP. Five main chemical functional groups of O-H, N-H, C=O, C-O, and C-H were detected in both materials whereas Fe-O was only found in CPF. The point of zero charges (pH_{pzc}) of CP and CPF were 4.47 and 4.83. For batch experiments, the optimum conditions of CP and CPF were 0.5 g, 4 h, pH 5, 50 mg/L and 0.3 g, 2 h, pH 5, 50 mg/L, and their lead removal efficiencies were 95.35 % and 99.57 %. As a result, CPF demonstrated a higher lead removal efficiency than CP because it spent less material dosage and contact time than CP. Thus, adding iron (III) oxide-hydroxide helped to improve material efficiency for lead adsorption. For the adsorption isotherm study, CP corresponded to the Langmuir model related to a physical adsorption process whereas CPF corresponded to the Freundlich model correlated to a physicochemical adsorption process. For the kinetic study, they corresponded to a pseudo-second-order kinetic model related to a chemisorption process with heterogeneous adsorption. Moreover, both CP and CPF could be reusable for more than 5 cycles for lead adsorption of more than 77 %. Therefore, CP and CPF were high-potential materials for lead adsorptions in an aqueous solution, and CPF demonstrated the highest lead removal efficiency. Therefore, CPF was suitable to apply for industrial wastewater treatment applications in the future.

For future works, the competing ions such as sodium (Na^+), and magnesium (Mg^{2+}), contaminated in real wastewater should be investigated to confirm the specific lead adsorption by CP or CPF, and the continuous flow study also needs to study for further industrial applications.

Funding

The authors are grateful for the financial support received from Research, Innovation and Academic Services Fund, Faculty of Science, Khon Kaen University.

CRedit authorship contribution statement

Pornsawai Praipipat: Supervision, Conceptualization, Funding acquisition, Investigation, Methodology, Validation, Formal analysis, Visualization, Writing – original draft, Writing – review & editing. **Pimploy Ngamsurach:** Visualization, Investigation, Writing – original draft. **Krissana Pratumkaew:** Investigation.

Declaration of Competing Interest

The authors declare that they have no known competing financial interests or personal relationships that could have appeared to influence the work reported in this paper.

References

- Ahmad, M., Usman, A.R.A., Lee, S.S., Kim, S.C., Joo, J.H., Yang, J.E., Ok, Y.S., 2012. Eggshell and coral wastes as low cost sorbents for the removal of Pb^{2+} , Cd^{2+} and Cu^{2+} from aqueous solutions. *J. Ind. Eng. Chem.* 18, 198–204. <https://doi.org/10.1016/j.jiec.2011.11.013>.
- Akram, A., Muzammal, S., Shakoor, M.B., Ahmad, S.R., Jilani, A., Iqbal, J., Al-Sehemi, A.G., Kalam, A., Aboushoushah, S.F.O., 2022. Synthesis and application of egg shell biochar for As(V) removal from aqueous solutions. *Catalysts* 12, 431. <https://doi.org/10.3390/catal12040431>.
- Alamillo-López, V.M., Sánchez-Mendieta, V., Olea-Mejía, O.F., González-Pedroza, M.G., Morales-Luckie, R.A., 2020. Efficient removal of heavy metals from aqueous solutions using a bio-nanocomposite of Eggshell/Ag-Fe. *Catalysts* 10, 727. <https://doi.org/10.3390/catal10070727>.
- Ali, H., Khan, E., Ilahi, I., 2019. Environmental chemistry and ecotoxicology of hazardous heavy metals: Environmental persistence, toxicity, and bioaccumulation. *J. Chem.* 2019, 6730305. <https://doi.org/10.1155/2019/6730305>.
- Alnasrawi, F.A.M., Kareem, S.L., Mohammed Saleh, L.A., 2022. Adsorption of methylene blue from aqueous solution using different types of activated carbon. *J. Appl. Water Eng. Res.* <https://doi.org/10.1080/23249676.2022.2120918>.
- Aryee, A.A., Mpatani, F.M., Du, Y., Kani, A.N., Dovi, E., Han, R., Li, Z., Qu, L., 2021. Fe_3O_4 and iminodiacetic acid modified peanut husk as a novel adsorbent for the uptake of Cu (II) and Pb (II) in aqueous solution: Characterization, equilibrium and kinetic study. *Environ. Pollut.* 268. <https://doi.org/10.1016/j.envpol.2020.115729>.
- Attia, N.F., El-Monaem, E.M.A., El-Aqapa, H.G., Elashery, S.E.A., Eltaweil, A.S., El Kady, M., Khalifa, S.A.M., Hawash, H.B., El-Seedi, H.R., 2022. Iron oxide nanoparticles and their pharmaceutical applications. *Appl. Surf. Sci. Adv.* 11. <https://doi.org/10.1016/j.apsadv.2022.100284>.
- Awogbemi, O., Inambao, F., Onuh, E.I., 2020. Modification and characterization of chicken eggshell for possible catalytic applications. *Heliyon* 6, e05283.
- Balali-Mood, M., Naseri, K., Tahergorabi, Z., Khazdair, M.R., Sadeghi, M., 2021. Toxic mechanisms of five heavy metals: mercury, lead, chromium, cadmium, and arsenic. *Front. Pharmacol.* 12. <https://doi.org/10.3389/fphar.2021.643972>.
- Basaleh, A.A., Al-Malack, M.H., Saleh, T.A., 2020. Metal removal using chemically modified eggshells: Preparation, characterization, and statistical analysis. *Desalin. Water Treat.* 173, 313–330. <https://doi.org/10.5004/dwt.2020.24690>.
- Basha, I.K., Abd El-Monaem, E.M., Khalifa, R.E., Omer, A.M., Eltaweil, A.S., 2022. Sulfonated graphene oxide impregnated cellulose acetate floated beads for adsorption of methylene blue dye: optimization using response surface methodology. *Sci. Rep.* 12, 9339. <https://doi.org/10.1038/s41598-022-13105-4>.
- Bayu, A.B., Abeto Amibo, T., Beyan, S.M., 2022. Adsorptive capacity of calcinated hen eggshell blended with silica gel for removal of lead II ions from aqueous media: kinetics and equilibrium studies. *J. Environ. Public Health* 2022, 2882546. <https://doi.org/10.1155/2022/2882546>.
- Boeykens, S.P., Redondo, N., Obeso, R.A., Caracciolo, N., Vázquez, C., 2019. Chromium and Lead adsorption by avocado seed biomass study through the use of Total Reflection X-Ray Fluorescence analysis. *Appl. Radiat. Isot.* 153. <https://doi.org/10.1016/j.apradiso.2019.108809>.
- Çelebi, H., Gök, G., Gök, O., 2020. Adsorption capability of brewed tea waste in waters containing toxic lead(II), cadmium (II), nickel (II), and zinc(II) heavy metal ions. *Sci. Rep.* 10, 17570. <https://doi.org/10.1038/s41598-020-74553-4>.
- Dubinina, M.M., Radushkevich, L.V., 1947. The equation of the characteristic curve of activated charcoal. *Proc. USSR Acad. Sci.* 55, 327–329.
- Elovich, S.Y., Larinov, O.G., 1962. Theory of adsorption from solutions of non electrolytes on solid (I) equation adsorption from solutions and the analysis of its simplest form, (II) verification of the equation of adsorption isotherm from solutions. *Izv. Akad. Nauk. SSSR. Otd. Khim. Nauk* 2, 209–216.
- Eltaweil, A.S., Abd El-Monaem, E.M., El-Subruiti, G.M., Ali, B.M., Abd El-Latif, M.M., Omer, A.M., 2022. Graphene oxide incorporated cellulose acetate beads for efficient removal of methylene blue dye; isotherms, kinetic, mechanism and co-existing ions studies. *J. Porous Mater.* <https://doi.org/10.1007/s10934-022-01347-6>.
- Freundlich, H., 1906. Over the adsorption in solution. *J. Phys. Chem.* 57, 385–470. <https://doi.org/10.1515/zpch-1907-5723>.
- Gaur, N., Kukreja, A., Yadav, M., Tiwari, A., 2018. Adsorptive removal of lead and arsenic from aqueous solution using soya bean as a novel biosorbent: equilibrium isotherm and thermal stability studies. *Appl. Water Sci.* 8, 98. <https://doi.org/10.1007/s13201-018-0743-5>.
- Gurav, V.L., Samant, R.A., 2021. Application of waste egg shell for adsorption of Cd(II) and Pb(II) ions to protect environment: equilibrium, kinetic and adsorption studies. *Orient. J. Chem.* 37, 128–135. <https://doi.org/10.13005/ojc/370117>.
- Hassan, E.S.R.E., Rostom, M., Farghaly, F.E., Abdel Khalek, M.A., 2020. Bio-sorption for tannery effluent treatment using eggshell wastes; kinetics, isotherm and thermodynamic study. *Egypt. J. Pet.* 29, 273–278. <https://doi.org/10.1016/j.ejpe.2020.10.002>.
- Ho, Y.S., McKay, G., 1999. Pseudo-second order model for sorption processes. *Process Biochem.* 34, 451–465. [https://doi.org/10.1016/S0032-9592\(98\)00112-5](https://doi.org/10.1016/S0032-9592(98)00112-5).
- Huang, Y., Gao, Y., Zhang, Q., Zhang, Y., Cao, J.J., Ho, W., Lee, S. C., 2018. Biocompatible FeOOH-Carbon quantum dots nanocomposites for gaseous NO_x removal under visible light: Improved charge separation and High selectivity. *J. Hazard. Mater.* 354, 54–62. <https://doi.org/10.1016/j.jhazmat.2018.04.071>.
- Jangkorn, S., Youngme, S., Praipipat, P., 2022. Comparative lead adsorptions in synthetic wastewater by synthesized zeolite A of recycled industrial wastes from sugar factory and power plant. *Heliyon* 8, e09323.

- Kasirajan, R., Bekele, A., Girma, E., 2022. Adsorption of lead (Pb-II) using CaO-NPs synthesized by sol-gel process from hen eggshell: Response surface methodology for modeling, optimization and kinetic studies. *South African J. Chem. Eng.* 40, 209–229. <https://doi.org/10.1016/j.sajce.2022.03.008>.
- Kayranli, B., 2022. Cadmium removal mechanisms from aqueous solution by using recycled lignocelluloses. *Alexandria Eng. J.* 61, 443–457. <https://doi.org/10.1016/j.aej.2021.06.036>.
- Kristianto, H., Dauly, N., Arie, A.A., 2019. Adsorption of Ni(II) ion onto calcined eggshells: a study of equilibrium adsorption isotherm. *Indones. J. Chem.* 19, 143–150. <https://doi.org/10.22146/ijc.29200>.
- Kumar, P.N., 2020. Experimental and kinetic study of removal of lead (Pb²⁺) from battery effluent using sweet lemon (*Citrus limetta*) peel biochar adsorbent. *Environ. Dev. Sustain.* 22, 4379–4406.
- Kyzas, G.Z., Mitropoulos, A.C., 2018. Zero-cost agricultural wastes as sources for activated carbons synthesis: lead ions removal from wastewaters. *Proc.* 2, 652. <https://doi.org/10.3390/proceedings2110652>.
- Lagergren, S., 1898. About the theory of so-called adsorption of soluble substances. *K. Sven. Vetenskapsakademiens Handl.* 24, 1–39.
- Langmuir, I., 1918. The adsorption of gases on plane surfaces of glass, mica and platinum. *J. Am. Chem. Soc.* 40, 1361–1403.
- Lulit, H., Natnael, S., Dure, M., Thriveni, T., Ramakrishna, C., Ji, W. A., 2019. Synthesis of nano-calcium oxide from waste eggshell by sol-gel method. *Sustainability* 11, 2–10.
- Mahdavi, S., Jalali, M., Afkhami, A., 2015. Heavy metals removal from aqueous solutions by Al₂O₃ nanoparticles modified with natural and chemical modifiers. *Clean Technol. Environ. Policy* 17, 85–102. <https://doi.org/10.1007/s10098-014-0764-1>.
- Mathangi, J.B., Helen Kalavathy, M., 2019. Study of mathematical models for the removal of Ni²⁺ from aqueous solutions using *Citrullus lanatus* rind, an agro-based waste. *Water Environ. J.* 33, 276–291. <https://doi.org/10.1111/wej.12408>.
- Maxwell, O.I., Onyebuchukwu, M.G., Ifechukwu, E.E., Onyejiwa, T. C., Oluchukwu, A.C., Margret, E.-E., 2020. Application of activated eggshell as effective adsorbent in the removal of lead (II) ion from fertilizer plant eEffluent. *J. Mater. Sci. Res. Rev.* 5, 18–36.
- Meng, D., Gong, X., Peng, Z., Wang, Z., Ren, D., 2022. Removal of Cd²⁺ in water by FeSO₄ magnetic modified eggshell adsorbent. *Desalin. Water Treat.* 247, 161–172. <https://doi.org/10.5004/dwt.2022.28048>.
- Mohammed, A.A., Al-Musawi, T.J., Kareem, S.L., Zarrabi, M., Al-Ma'abreh, A.M., 2020. Simultaneous adsorption of tetracycline, amoxicillin, and ciprofloxacin by pistachio shell powder coated with zinc oxide nanoparticles. *Arab. J. Chem.* 13, 4629–4643. <https://doi.org/10.1016/j.arabjc.2019.10.010>.
- Mohammed, A.A., Kareem, S.L., 2021. Enhancement of ciprofloxacin antibiotic removal from aqueous solution using zno nanoparticles coated on pistachio shell. *Desalin. Water Treat.* 213, 229–239. <https://doi.org/10.5004/dwt.2021.26674>.
- Mohseni, E., Rostami, E., Hamdi, Z., Mehrizi, M.M., Rahmani, A., 2022. The effect of activated carbon produced from remnants of walnut shell and ox tongue leftover on removing cadmium metal from water. *Desalin. Water Treat.* 256, 176–193. <https://doi.org/10.5004/dwt.2022.28410>.
- Naghizadeh, M., Taher, M.A., Nejad, L.Z., Moghaddam, F.H., 2018. Fabrication, characterization and theoretical investigation of novel Fe₃O₄@egg-shell membrane as a green nanosorbent for simultaneous preconcentration of Cu (II) and Tl (I) prior to ETAAS determination. *Environ. Nanotechnol. Monit. Manage.* 10, 171–178. <https://doi.org/10.1016/j.enmm.2018.06.001>.
- Ngamsurach, P., Namwongsa, N., Praipipat, P., 2022a. Synthesis of powdered and beaded chitosan materials modified with ZnO for removing lead (II) ions. *Sci. Rep.* 12, 17184. <https://doi.org/10.1038/s41598-022-22182-4>.
- Ngamsurach, P., Nemkhuntod, S., Chanaphan, P., Praipipat, P., 2022b. Modified beaded materials from recycled wastes of bagasse and bagasse fly ash with iron (III) oxide-hydroxide and zinc oxide for the removal of reactive blue 4 dye in aqueous solution. *ACS Omega* 7, 34839–34857. <https://doi.org/10.1021/acsomega.2c03250>.
- Ngamsurach, P., Praipipat, P., 2021. Modified alginate beads with ethanol extraction of *Cratogeomys formosum* and *Polygonum odoratum* for antibacterial activities. *ACS Omega* 6, 32215–32230. <https://doi.org/10.1021/acsomega.1c05056>.
- Ngamsurach, P., Praipipat, P., 2022a. Antibacterial activities against *Staphylococcus aureus* and *Escherichia coli* of extracted *Piper betle* leaf materials by disc diffusion assay and batch experiments. *RSC Adv.* 12, 26435–26454. <https://doi.org/10.1039/d2ra04611c>.
- Ngamsurach, P., Praipipat, P., 2022b. Comparative antibacterial activities of *Garcinia cowa* and *Piper sarmentosum* extracts against *Staphylococcus aureus* and *Escherichia coli* with studying on disc diffusion assay, material characterizations, and batch experiments. *Heliyon* 8, e11704.
- Novoseltseva, V., Yankovych, H., Kovalenko, O., Václavíková, M., Melnyk, I., 2021. Production of high-performance lead(II) ions adsorbents from pea peels waste as a sustainable resource. *Waste Manag. Res.* 39, 584–593. <https://doi.org/10.1177/0734242X20943272>.
- Obeng-Gyasi, E., 2019. Sources of lead exposure in various countries. *Rev. Environ. Health* 34, 25–34. <https://doi.org/10.1515/reveh-2018-0037>.
- Peigneux, A., Puentes-Pardo, J.D., Rodríguez-Navarro, A.B., Hincke, M.T., Jimenez-Lopez, C., 2020. Development and characterization of magnetic eggshell membranes for lead removal from wastewater. *Ecotoxicol. Environ. Saf.* 192, . <https://doi.org/10.1016/j.ecoenv.2020.110307> 110307.
- Praipipat, P., Ngamsurach, P., Prasongdee, V., 2022a. Comparative reactive blue 4 dye removal by lemon peel bead doping with iron (III) oxide-hydroxide and zinc oxide. *ACS Omega* 7, 41744–41758. <https://doi.org/10.1021/acsomega.2c05956>.
- Praipipat, P., Ngamsurach, P., Roopkhan, N., 2023. Zeolite A powder and beads from sugarcane bagasse fly ash modified with iron(III) oxide-hydroxide for lead adsorption. *Sci. Rep.* 13, 1873. <https://doi.org/10.1038/s41598-023-29055-4>.
- Praipipat, P., Ngamsurach, P., Saekrathok, C., Phomtai, S., 2022b. Chicken and duck eggshell beads modified with iron (III) oxide-hydroxide and zinc oxide for reactive blue 4 dye removal. *Arab. J. Chem.* 15, . <https://doi.org/10.1016/j.arabjc.2022.104291> 104291.
- Praipipat, P., Ngamsurach, P., Kosumphon, S., Mokkarat, J., 2023a. Powdered and beaded sawdust materials modified iron (III) oxide-hydroxide for adsorption of lead (II) ion and reactive blue 4 dye. *Sci. Rep.* 13, 531. <https://doi.org/10.1038/s41598-023-27789-9>.
- Praipipat, P., Ngamsurach, P., Sanghuayprai, A., 2023b. Modification of sugarcane bagasse with iron(III) oxide-hydroxide to improve its adsorption property for removing lead(II) ions. *Sci. Rep.* 13, 1467. <https://doi.org/10.1038/s41598-023-28654-5>.
- Praipipat, P., Ngamsurach, P., Thanyahan, A., Sakda, A., 2023c. Reactive blue 4 adsorption efficiencies on bagasse and bagasse fly ash beads modified with titanium dioxide (TiO₂), magnesium oxide (MgO), and aluminum oxide (Al₂O₃). *Ind. Crop. Prod.* 191, . <https://doi.org/10.1016/j.indcrop.2022.115928> 115928.
- Qasem, N.A.A., Mohammed, R.H., Lawal, D.U., 2021. Removal of heavy metal ions from wastewater: a comprehensive and critical review. *npj Clean Water* 4. <https://doi.org/10.1038/s41545-021-00127-0>.
- Rahmani-Sani, A., Singh, P., Raizada, P., Claudio Lima, E., Anastopoulos, I., Giannakoudakis, D.A., Sivamani, S., Dontsova, T.A., Hosseini-Bandegharai, A., 2020. Use of chicken feather and eggshell to synthesize a novel magnetized activated carbon for sorption of heavy metal ions. *Bioresour. Technol.* 297, . <https://doi.org/10.1016/j.biortech.2019.122452> 122452.
- Razzaz, A., Ghorban, S., Hosayni, L., Irani, M., Aliabadi, M., 2016. Chitosan nanofibers functionalized by TiO₂ nanoparticles for the

- removal of heavy metal ions. *J. Taiwan Inst. Chem. Eng.* 58, 333–343. <https://doi.org/10.1016/j.jtice.2015.06.003>.
- Rouquerol, J., Avnir, D., Fairbridge, C.W., Everett, D.H., Haynes, J. M., Pernicone, N., Ramsay, J.D.F., Sing, K.S.W., Unger, K.K., 1994. Recommendations for the characterization of porous solids (Technical report). *Pure Appl. Chem.* 66, 1739–1758. <https://doi.org/10.1351/pac199466081739>.
- Soares, M.A.R., Marto, S., Quina, M.J., Gando-Ferreira, L., Quinta-Ferreira, R., 2016. Evaluation of eggshell-rich compost as biosorbent for removal of Pb(II) from aqueous solutions. *Water. Air. Soil Pollut.* 227, 150. <https://doi.org/10.1007/s11270-016-2843-x>.
- Tejada-Tovar, C., Gonzalez-Delgado, A.D., Villabona-Ortiz, A., 2019. Characterization of residual biomasses and its application for the removal of lead ions from aqueous solution. *Appl. Sci.* 9, 4486. <https://doi.org/10.3390/app9214486>.
- Temkin, M.I., Pyzhev, V., 1940. Kinetics of ammonia synthesis on promoted iron catalysts. *Acta physiochim. URSS* 12, 327–356.
- Threpanich, A., Praipipat, P., 2021. Powdered and beaded lemon peels-doped iron (III) oxide-hydroxide materials for lead removal applications: Synthesis, characterizations, and lead adsorption studies. *J. Environ. Chem. Eng.* 9, <https://doi.org/10.1016/j.jece.2021.106007> 106007.
- Threpanich, A., Praipipat, P., 2022. Efficacy study of recycling materials by lemon peels as novel lead adsorbents with comparing of material form effects and possibility of continuous flow experiment. *Environ. Sci. Pollut. Res.* 29, 46077–46090. <https://doi.org/10.1007/s11356-022-19131-z>.
- Tizo, M.S., Blanco, L.A.V., Cagas, A.C.Q., Dela Cruz, B.R.B., Encoy, J.C., Gunting, J.V., Arazo, R.O., Mabayo, V.I.F., 2018. Efficiency of calcium carbonate from eggshells as an adsorbent for cadmium removal in aqueous solution. *Sustain. Environ. Res.* 28, 326–332. <https://doi.org/10.1016/j.serj.2018.09.002>.
- Wang, G., Liu, N., Zhang, S., Zhu, J., Xiao, H., Ding, C., 2022. Preparation and application of granular bentonite-eggshell composites for heavy metal removal. *J. Porous Mater.* 29, 817–826. <https://doi.org/10.1007/s10934-022-01208-2>.
- Weber, W.J., Morris, J.C., 1963. Kinetics of adsorption carbon from solution. *J. Sanit. Eng. Div.* 89, 31–60.
- Xu, W., Lan, H., Wang, H., Liu, H., Qu, J., 2015. Comparing the adsorption behaviors of Cd, Cu and Pb from water onto Fe-Mn binary oxide, MnO₂ and FeOOH. *Front. Environ. Sci. Eng.* 9, 385–393. <https://doi.org/10.1007/s11783-014-0648-y>.